Ion Microprobe Dating of Zircons from Heikongshan Volcano (Tengchong Volcanic Field, Southeast Tibetan Plateau): Time Scales and Nature of Magma Storage

by

Yang Peng

A thesis submitted to the Graduate Faculty of
Auburn University
in partial fulfillment of the
requirements for the Degree of
Master of Science

Auburn, Alabama
August 4, 2012

Approved by

Haibo Zou, Chair, Assistant Professor of Geology and Geography
Willis E. Hames, Professor of Geology and Geography
David T. King, Jr., Professor of Geology and Geography
Mark G. Steltenpohl, Professor of Geology and Geography

Abstract

Although Cenezoic post-collisional volcanism is widespread on the Tibetan Plateau, young volcanoes suitable for studying the timescales of magma chamber processes are rather rare. Three young potassic volcanoes (Maanshan, Dayingshan, and Heikongshan) from the Tengchong area, southeast Tibetan Plateau, have been reported with eruption ages of less than 10 ka. The potassic lavas contain information about melt generation and magma chamber processes underneath the Tibetan Plateau. There is now a general consensus that pre-eruption zircon growth can be used to constrain the time scales of magma chamber processes. In the present study, we utilize a secondary ion mass spectrometry to measure U-Th zircon ages from the Heikongshan volcano to estimate magma residence times.

The U-Th ages of zircon yielded ages of 67.3 ± 14 ka and 99.9 ± 4.6 ka, which represent two stages of zircon crystallization. Using an eruption age of < 10 ka, the zircon storage time in the magma chamber is at least 57.3 ka. Combining geochemical analysis with previous geologic study in the Tengchong area, the Heikongshan magma is probably derived from partial melting of an enriched mantle metasomatized by fluids from previous north-dipping subduction. This study will contribute to a broader understanding of the behavior and hazard of the Tengchong volcanic system.

Acknowledgments

This research was supported by National Science Foundation (NSF) grants (EAR 0917651 and EAR 1119077 to Zou). Axel Schmitt is thanked for providing guidance and instruction on the operation of the Secondary Ion Mass Spectrometry (SIMS) at the NSF National Ion Microprobe Facility at the University of California, Los Angeles (UCLA). I thank the GeoAnalytical Lab at Washington State University for the measurement of whole-rock major and trace element concentrations. Special thanks go to Haibo Zou for providing the funding, assistance in sample preparation, instruction on the operation of SIMS, and help in thesis writing. I also benefited from valuable suggestions and comments provided by thesis committee members Willis E. Hames, David T. King, Jr., and Mark G. Steltenpohl.

Thanks also go to my friends and colleagues at Auburn University who have provided so much wonderful feedback and help. They include Mitchell Moore, Ross Thomas Tucker, Sonnet Gomes, and Jonny Prouty.

Many other people have helped me in various ways. They include Lorraine W. Wolf, Ashraf Uddin, Ronald D. Lewis, and Charles E. Savrda at Auburn University and Qicheng Fan from Institute of Geology, China Earthquake Administration. My apologies to anyone I may have omitted.

Table of Contents

List of Tables

List of Figures

Introduction

Volcanism at the Tengchong volcanic field (TVF), southeast Tibetan Plateau, began long after the Indo-Asian collision and has continued to the present-day (Wang et al., 2006). The Tengchong volcanic field is the only part of the Himalayan geothermal belt that erupted during the Quaternary period in spite of widespread Cenozoic (<65 Ma) post-collisional potassic volcanism on the Tibetan Plateau (e.g., Deng, 1978; Turner et al., 1996; Flower et al., 1998; Miller et al., 1999; Ding et al., 2003). Three young potassic volcanoes (Maanshan, Dayingshan, and Heikongshan) in the Tengchong area, southeast Tibetan Plateau, have been reported with the eruption ages less than 10 ka. The potassic lavas contain unique information about melt generation and magma chamber processes, such as time scales of pre-eruption magma residence, underneath the Tibetan Plateau (Zou et al., 2010). Constraints on magma residence times contribute to a broader understanding of the behavior of volcanic systems and are useful for volcanic hazard assessment.

The time scales of pre-eruption magma residence can be inferred from the difference between eruption age and zircon crystallization age (Reid et al., 1997). There is now a general consensus that pre-eruption zircon growth can be used to constrain magma process time scales. Because it becomes more difficult to resolve absolute age difference as time goes on, relatively young eruptions can provide the most useful and

robust information about residence time scales (Simon et al., 2008). Fortunately, the eruption ages of Maanshan, Dayingshan and Heikongshan are very young (less than 10 ka), and they do contain zircon crystals, which makes these volcanic rocks suitable for studying the magma pre-eruptive history and conditions.

U-Th dating of zircon crystals is a highly effective dating tool, because uranium-series disequilibria have high absolute age resolution for short time scales (Fukuoka, 1974; Zou et al., 2010). Zircons in a magma body begin to crystallize or recrystallize in the magma prior to eruption. During its crystallization, zircons incorporate more U relative to Th into the zircon lattice (Fukuoka and Kigoshi, 1974; Pyle et al., 1988; Reid et al., 1997; Condomines, 1997; Blundy and Wood, 2003). Furthermore, diffusion of U and Th in zircon is slow (Cherniak et al., 1997). These two features enable zircons to preserve their U-Th crystallization ages (Reid et al., 1997).

Of the three Holocene volcanoes from Tengchong, Zou et al. (2010) worked on the Maanshan volcano and Tucker (2011) studied the Dayingshan volcano. They inferred magma storage times of Maanshan and Dayingshan are about 45 ka and 48 ka, respectively. Both volcanoes also contain an older population of zircons of 90 ka.

In this study, the focus is the Heikongshan volcano. U-Th data of zircons and major and trace element data from the Heikongshan volcano are presented to quantify magma storage time before eruption, and to place better constraints on the magma evolution of the Holocene Heikongshan volcanic rocks.

Objectives

Although the Heikongshan volcanic rocks have SiO_2 content (54%) lower than both Maanshan (57%) and Dayingshan (61%), which means it may contains less zircons than these two volcanoes, enough zircon grains were picked out from the fresh Heikongshan volcanic rocks for this study. Secondary ion mass spectrometry (SIMS) was used to analyze U and Th isotopes in zircon crystals. The U-Th data of zircons and major and trace element from Heikongshan volcano are presented in order to complete the following two objectives:

(1) determine the ages of zircons from the Heikongshan volcanic rocks in order to place constraints on the time scales of magma chamber processes; and

(2) place constraints on the magma generation and evolution of the Heikongshan volcanic rocks.

BACKGROUND

Geologic Setting

Tengchong volcanic field (TVF) (Fig. 1) is located along the southeastern margin of the Tibetan Plateau near the border between China and Burma. The gneissic basement underlying that region is known as the 'Tengchong block' and it is usually considered the southeastern part of the Himalayan fold zone or part of the Sundaland plate (Fan, 1978; Powell and Johnson, 1980). From Burma to Tengchong, there is a series of north-south-trending faults and sutures that developed in response to the collision between the Indian and Eurasian plates (Fig. 2). The Tengchong block is bordered by two north-south-trending strike-slip faults, the Sagaing Fault to the west and the Jinsha-Red River Fault to the east. To the south of the volcanic field are two active east-west-trending strike-slip faults (Fig. 2).

Volcanism at Tengchong began at approximately 5 Ma, long after the onset of the Indo-Eurasia collision (65 Ma), and has continued to the present, spanning the entire Quaternary period (Zhu et al., 1983; Wang et al., 2006). The area of the Tengchong volcanic field is about 600 km^2. There are 68 volcanoes and several hot springs in the Tengchong area. Among these volcanoes, 25 volcanic centers have well-preserved volcanic structures. Volcanic eruptions migrated to the central part (around Heikongshan,

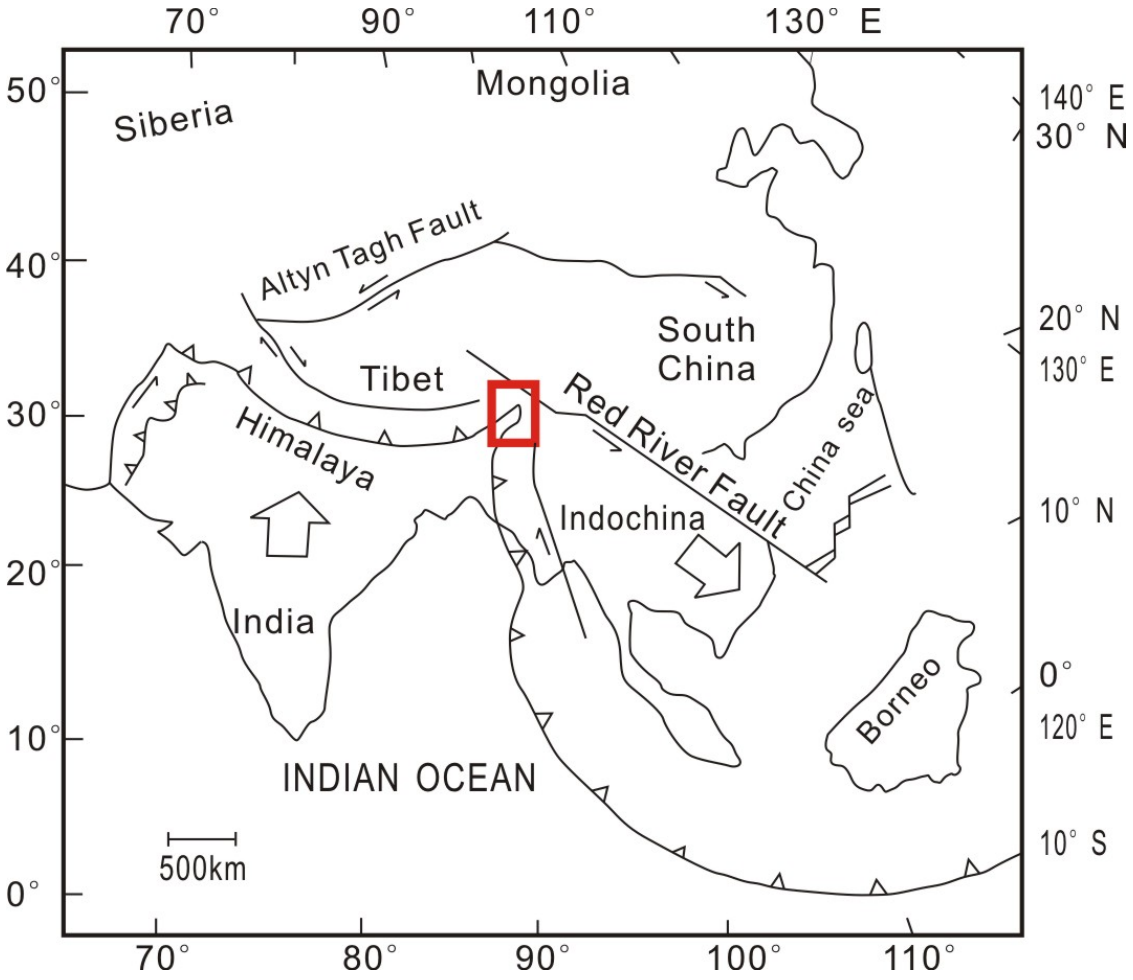

Figure 1. Regional map showing major tectonic features in Asia (after Tapponnier et al., 1990 and Zou et al., 2010). The Tengchong area is within the red box.

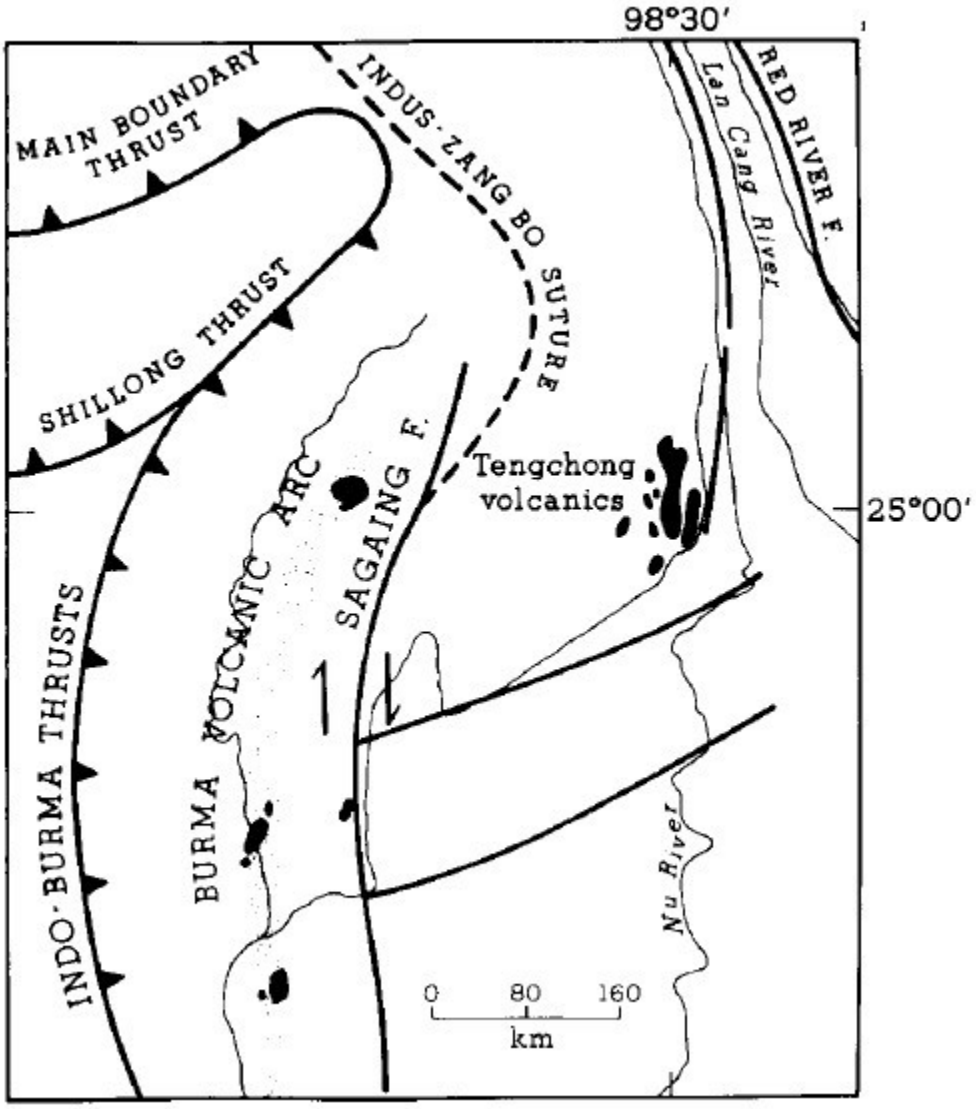

Figure 2. Map showing the location of the Tengchong volcanic field and regional tectonic features (After Zhu et al., 1983). The black areas indicate Cenozoic to recent volcanic fields.

Dayingshan and Maanshan) during the Pleistocene and Holecene from the southeastern and northwestern ends of the Tengchong volcanic field (Li et al., 2000) (Fig.3).

The dominant rock type of TVF is basalt. A minor portion of the volcanic rocks, which are the younger lavas, consists of basaltic andesites and andesitic dacites. These lavas are potassium rich. Wang et al. (2006) measured the major and trace element concentrations of some samples from these lavas, and reported that they plot within the high-K and calc-alkaline field.

Heikongshan volcano is located about 25 km north of Tengchong City (98° 30' E, 25° 13.8'N) and has an elevation of 2072 m (Yu et al., 2010). It is one of the most well-preserved volcanoes in the Tengchong Volcanic Field. The composite volcanic cone is composed of lavas and volcanic debris. The crater rim is reasonably well preserved. From the middle Pleistocene, the Heikongshan volcano began to erupt discontinuously several times (Li at al., 2000). There are at least four units of large-scale lava flows effused from the cone toward the west, north and east (Fig. 4) (Yu et al., 2010). The last eruption K-Ar age is 7.0 ± 7.0 ~ 14.0 ± 7.0 ka (Liu, 2000). The rocks of the Heikongshan lava flows have been categorized as trachyandesite by Fan (1978) and have high-K calc-alkaline compositions.

The Heikongshan samples contain a minor amount of mafic and ultramafic autoliths which are all smaller than 2.5 cm. Different sizes and shapes of vesicles are well developed in the lava. The samples have a porphyritic texture, containing about 8% to 10% phenocrysts of mainly plagioclase, pyroxene and olivine. Plagioclase phenocrysts are euhedral tabular crystals, and some have well-developed compound twining. The groundmass of the lava consists of small crystals (plagioclase, pyroxene and olivine) and

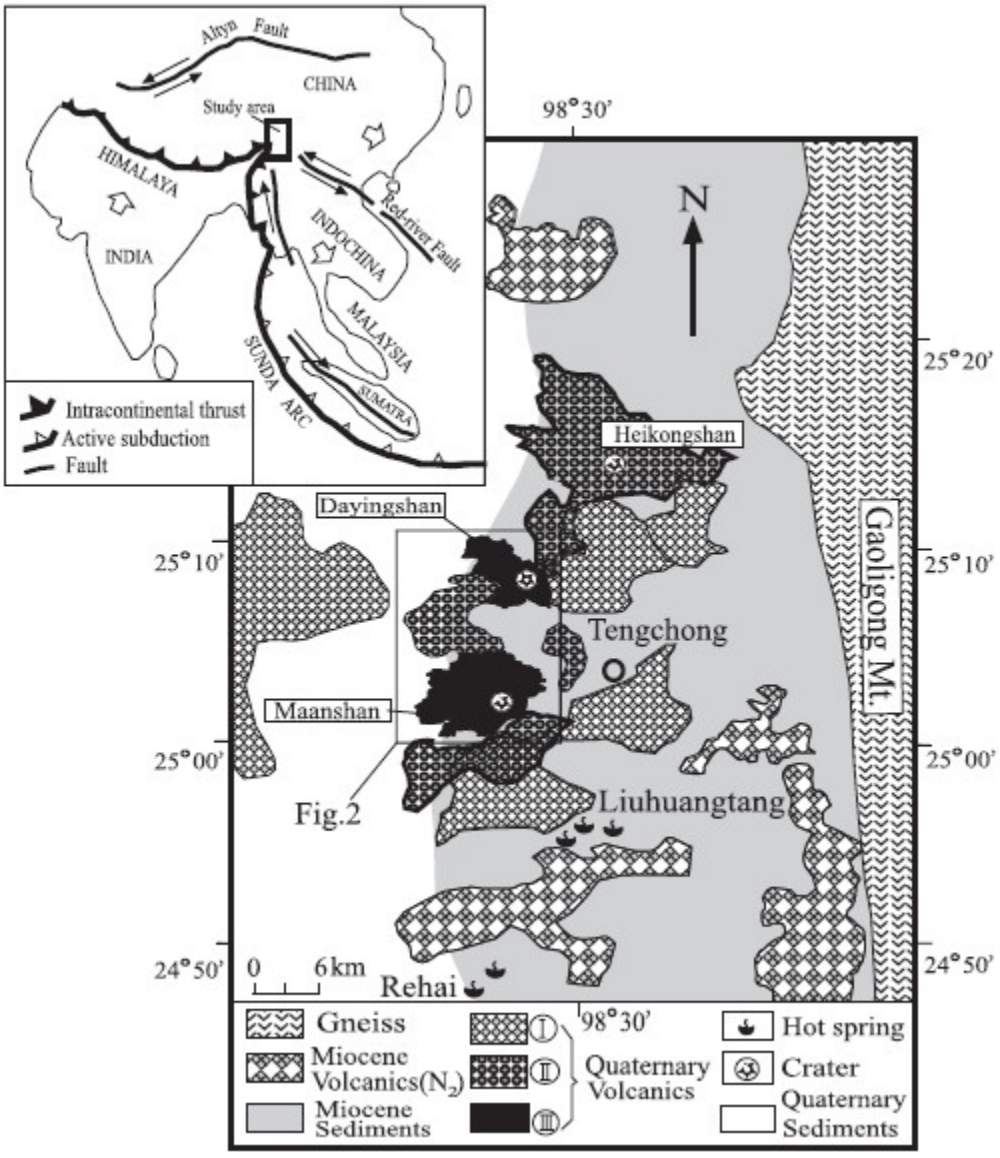

Figure 3. Distribution of the three Holocene volcanoes (Heikongshan, Dayingshan and Maanshan) and surrounding rocks (From Wang et al., 2006).

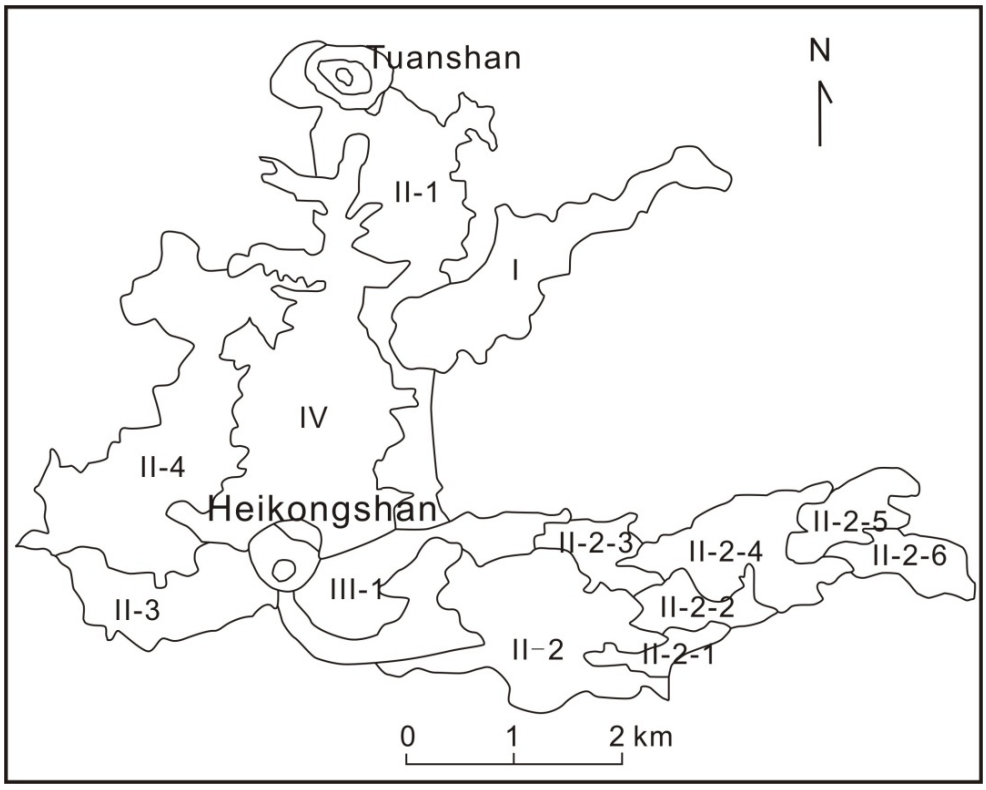

Figure 4. Map showing the division of lava flow units of Heikongshan volcano (after Yu et al., 2010).

volcanic glass (Figs. 5 and 6).

U-Th Disequilibrium Dating

U-Th disequilibrium refers to the disequilibrium between ^{238}U and its radiogenic daughter isotope ^{230}Th. ^{238}U decays to stable ^{206} Pb via a series of short-lived intermediate daughter isotopes with different half-lives (Fig. 7). Among these intermediate decay series, there are several short-lived decay series that can be utilized to date recent geologic processes. The half-life of ^{230}Th is 75,000 years, which is the longest of them.

If a geological system remains undisturbed for 375,000 years (five half-lives of ^{230}Th), the system reaches ^{238}U-^{230}Th secular equilibrium. During secular equilibrium, the decay rate of ^{238}U is the same as that of ^{230}Th ($\lambda_{238}{}^{238}U = \lambda_{230}{}^{230}Th$, λ is the decay constant). If a geological system was disturbed by some geologic events, such as partial melting, the secular equilibrium will not last and U-Th disequilibrium will occur. The extent of U-Th disequilibrium produced by partial melting is a function of elemental partition coefficients, melting porosity, melting rate and melting time (Zou, 2007). In 375,000 years (five half-lives of ^{230}Th) (Fig. 8), the system will return to secular equilibrium. The U-Th dating is essentially utilizing the characteristic of short-term U-Th disequilibrium to investigate the geological processes, which took place over the past 375,000 years.

Crystallization ages of young (<375,000 years) zircons can be determined by analyzing U and Th nuclide abundance and variation in U/Th. ^{230}Th is a daughter isotope

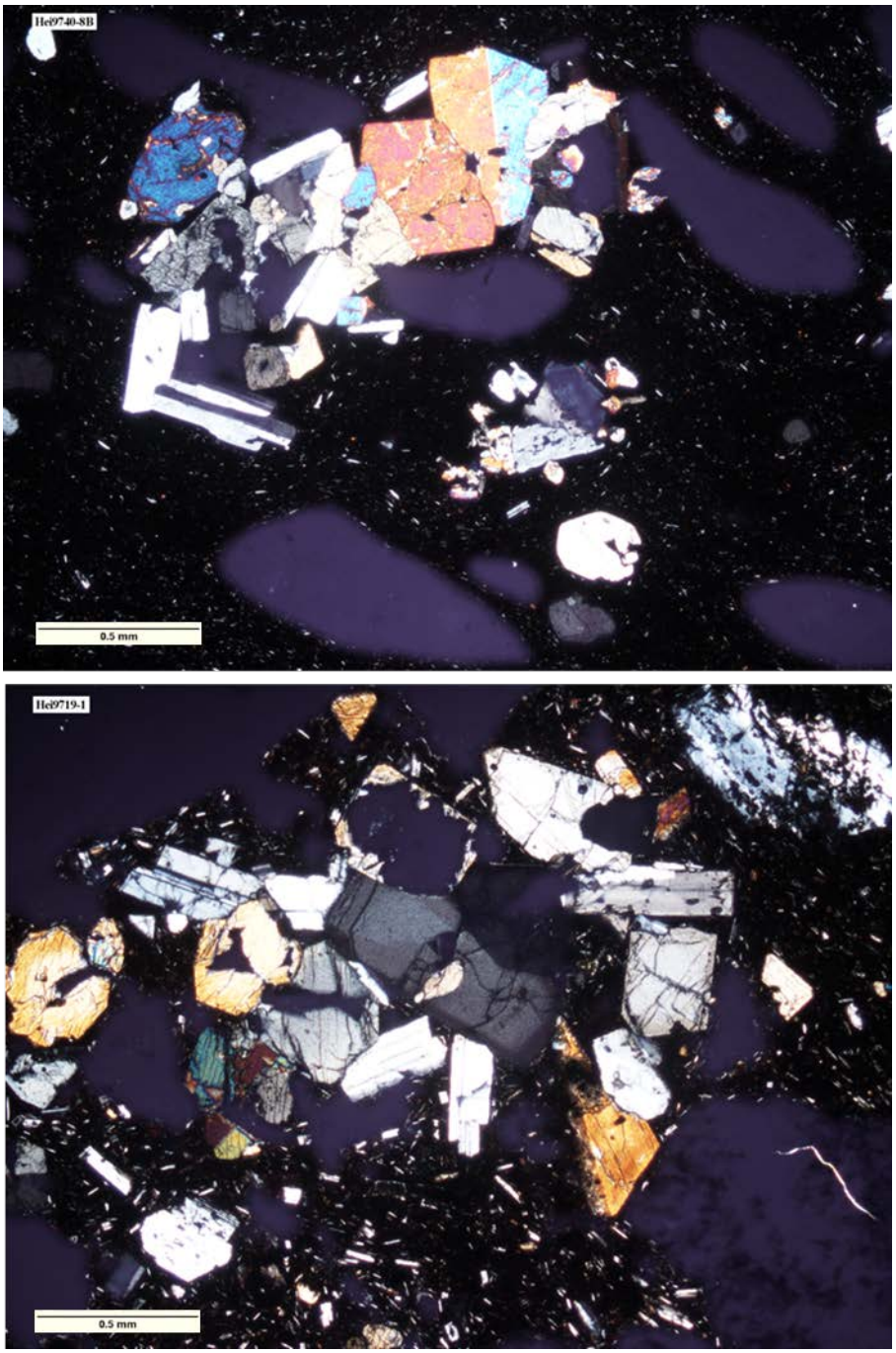

Figure 5. Photomicrographs of autoliths under crossed-polarized light (XPL) in Heikongshan volcanic rocks.

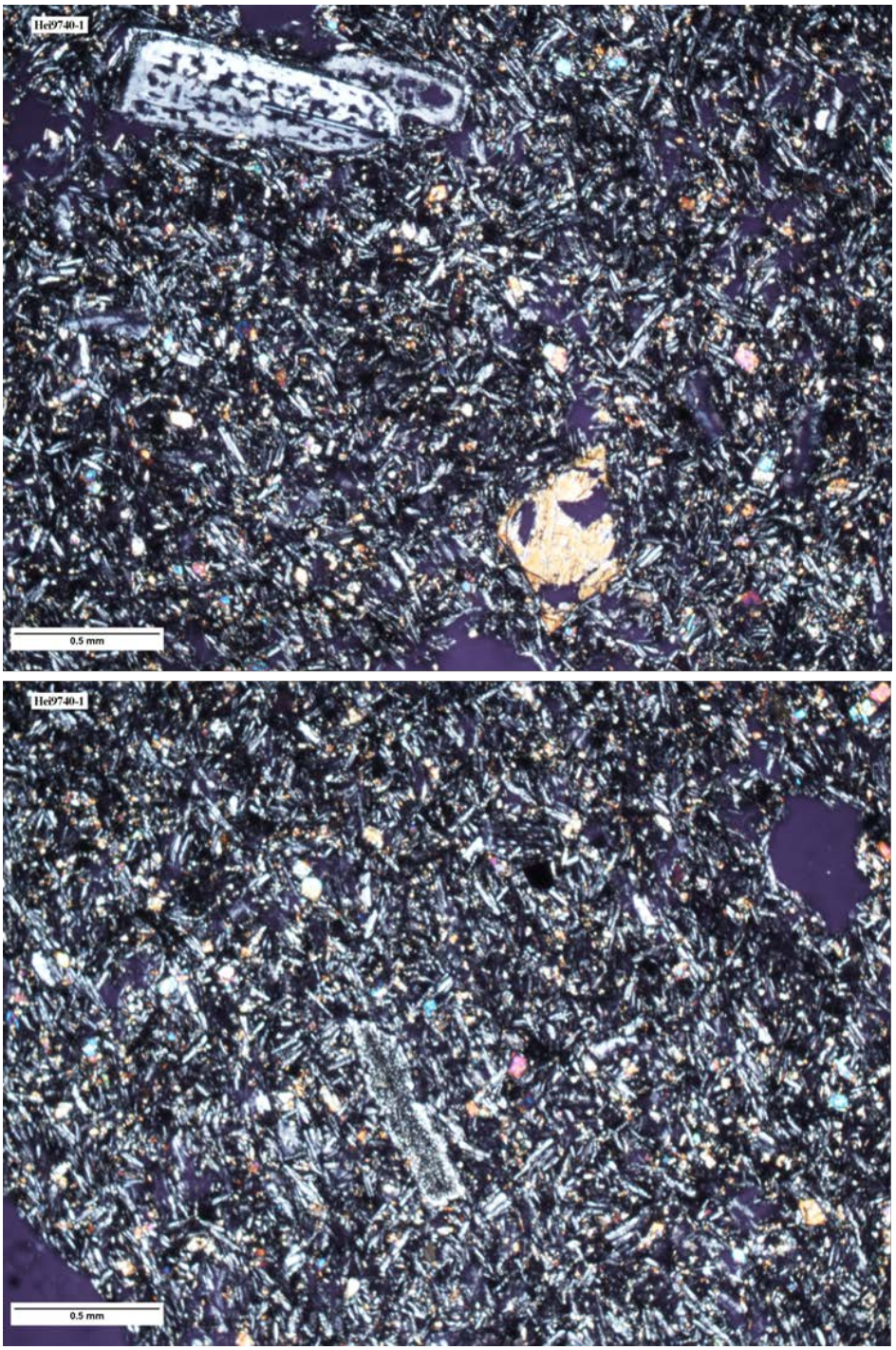

Figure 6. Photomicrographs of groundmass under crossed-polarized light (XPL) in Heikongshan volcanic rocks.

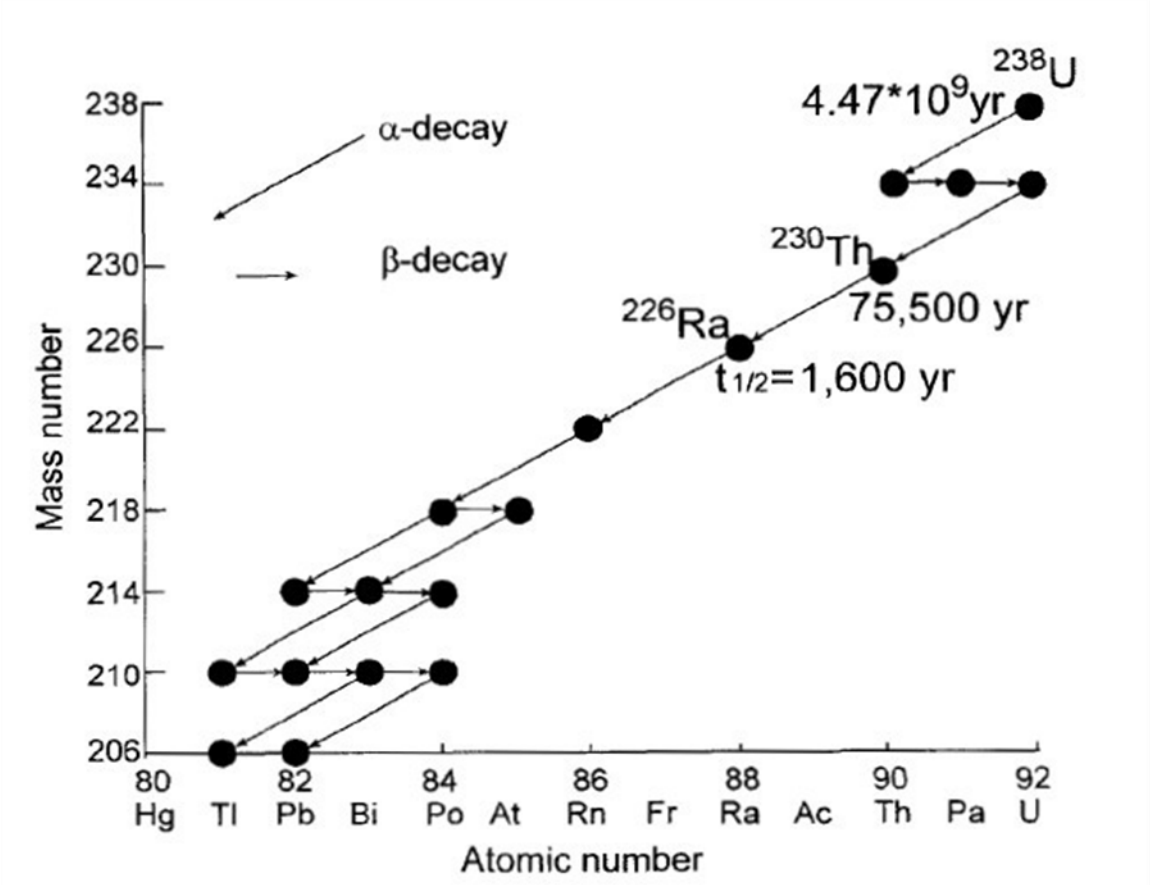

Figure 7. Schematics showing the decay series of ^{238}U to final stable ^{206}Pb. Among the intermediate isotopes, ^{230}Th can be used to investigate short-term recent geologic processes (From Zou, 2007).

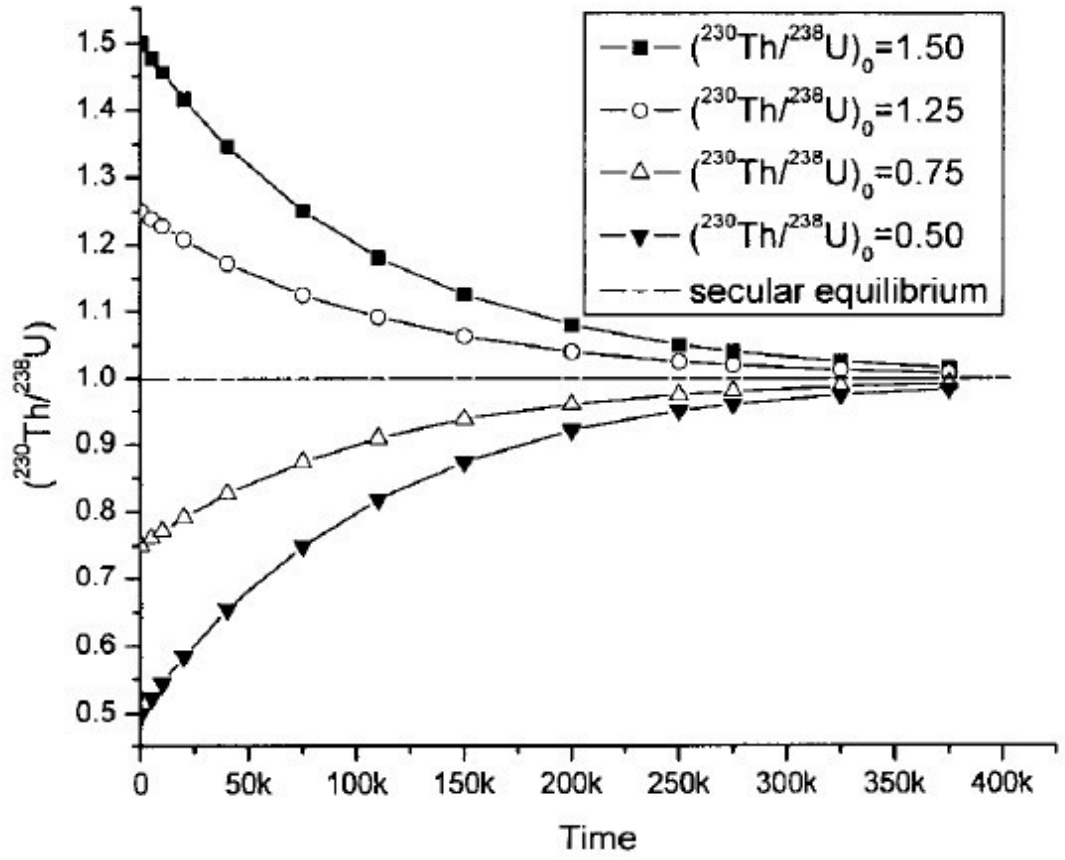

Figure 8. Evolution of (^{230}Th/^{238}U) with time for different initial (^{230}Th/^{238}U) ratios. Within 375,000 years, the system returns to secular equilibrium with (^{230}Th/^{238}U) =1.0 (From Zou, 2007).

of ^{238}U. During the crystallization period of zircon from a melt, ^{230}Th can be accumulated at different rates. If the zircon crystalized rapidly, a linear isochron will result on a plot of $^{238}U/^{232}Th$ versus $^{230}Th/^{232}Th$, with slope proportional to crystal age and an intercept to the equiline (Fig. 9). The equiline, representing secular equilibrium, equals to the initial $^{230}Th/^{232}Th$ of the crystal (and presumably magma) (Lowenstern et al., 2000). The ^{238}U-^{230}Th isochron can be constructed by the following equation:

$$\frac{\left(^{230}Th\right)}{\left(^{232}Th\right)} = \frac{\left(^{238}U\right)}{\left(^{232}Th\right)}\left(1 - e^{-\lambda_{230}t}\right) + \frac{\left(^{230}Th\right)^{0}}{\left(^{232}Th\right)}e^{-\lambda_{230}t}.$$

Then the age can be defined by isochron slope (m) of the line using the following equation:

$$t = \frac{1}{\lambda}\ln\left(\frac{1}{1-m}\right),$$

where λ is decay constant, and t is crystallization age of zircon.

Zircon Analysis by Secondary Ion Mass Spectrometry (SIMS)

Secondary Ion Mass Spectrometry (SIMS) (Fig. 10) is the surface analysis technique used to measure the chemical and isotopic composition of solid surfaces by sputtering the surface of the specimen with a focused primary ion beam and collecting and analyzing ejected secondary ions. High energy ions are supplied by an ion gun (Cesium ion source or Duoplasmatron) and focused on to the target sample, which ionizes and sputters some atoms off the surface (Fig. 11). These secondary ions are then collected by ion lenses and filtered according to atomic mass, then projected onto the ion detection unit (electron multiplier or detector). SIMS is one of the most

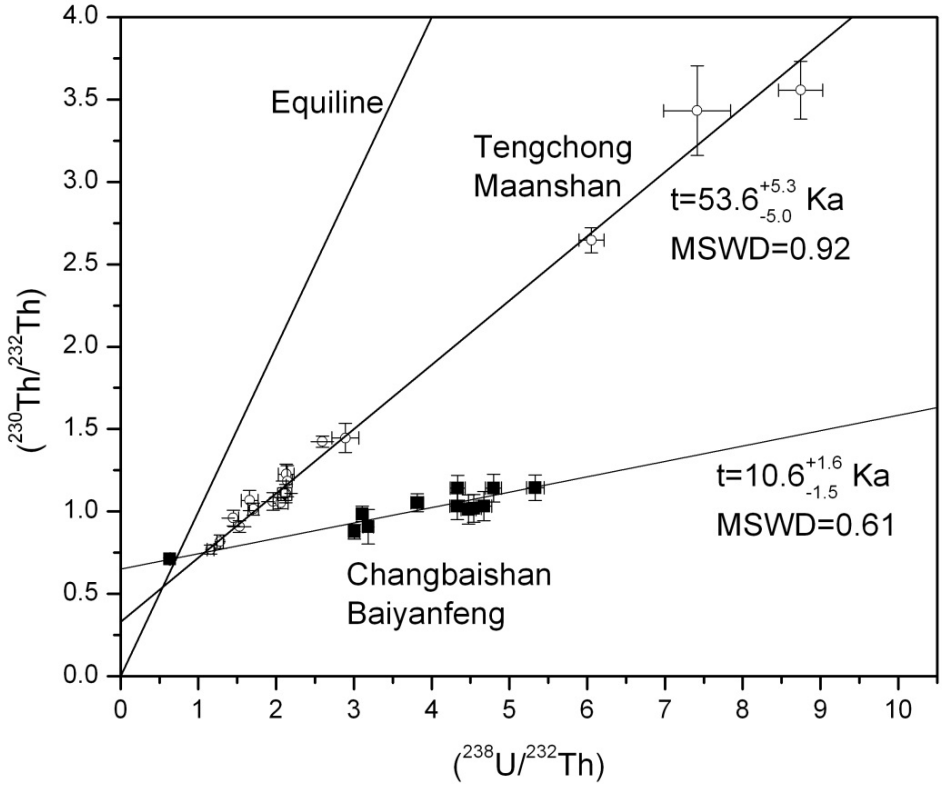

Figure 9. Zircon U-Th isochron for Tianchi volcano of Changbaishan and zircon surface U-Th isochron for Maanshan volcano of Tengchong (Zou and Fan, 2011). Note that the slopes of lines are proportional to zircon crystal ages.

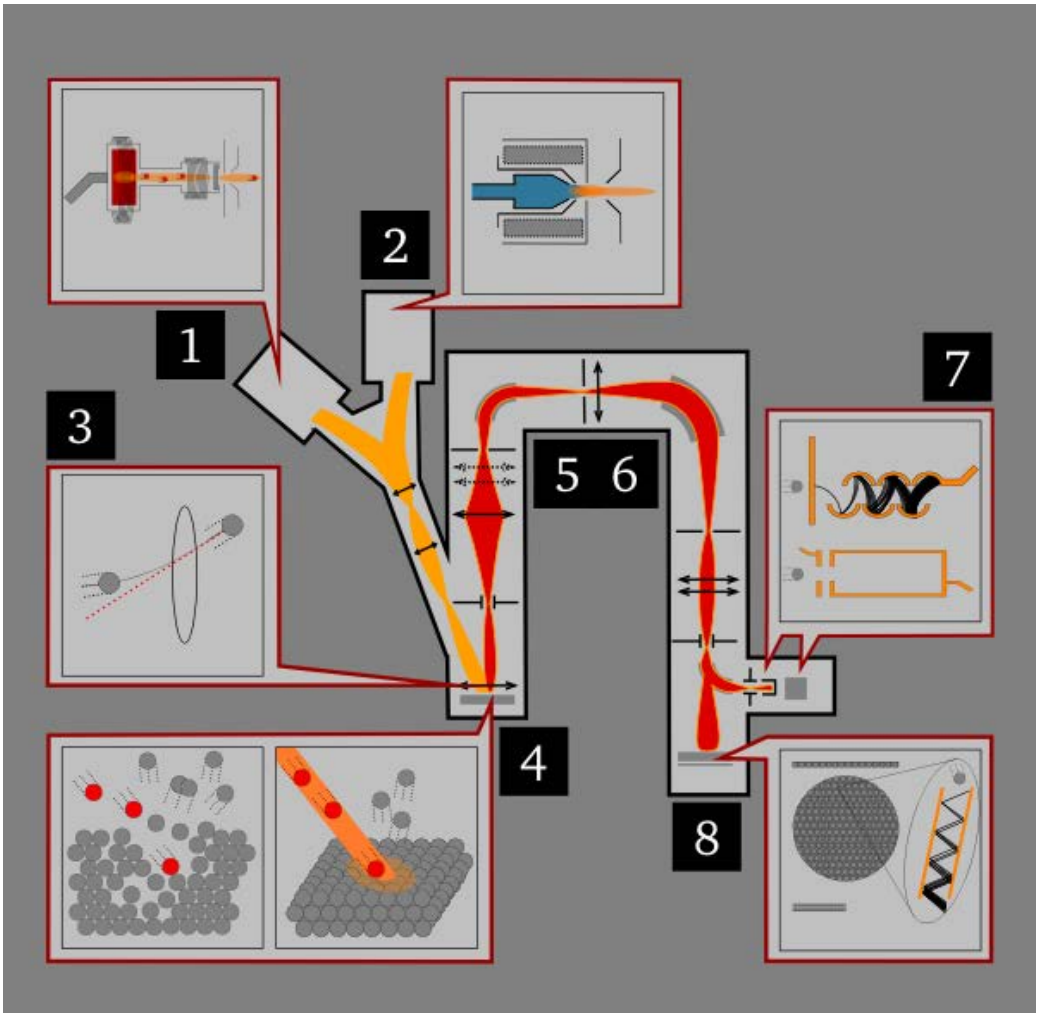

Figure 10. Diagram shows typical schematic of a dynamic SIMS instrument. 1: Cesium ion source; 2: Duoplasmatron; 3: Electrostatic lens; 4: Sample; 5: Electrostatic sector-ion energy analyser; 6: Electromagnet-mass analyser; 7: Electron multiplier/Faraday cup; 8: Channel-plate/Fluorescent screen-ion image detector.

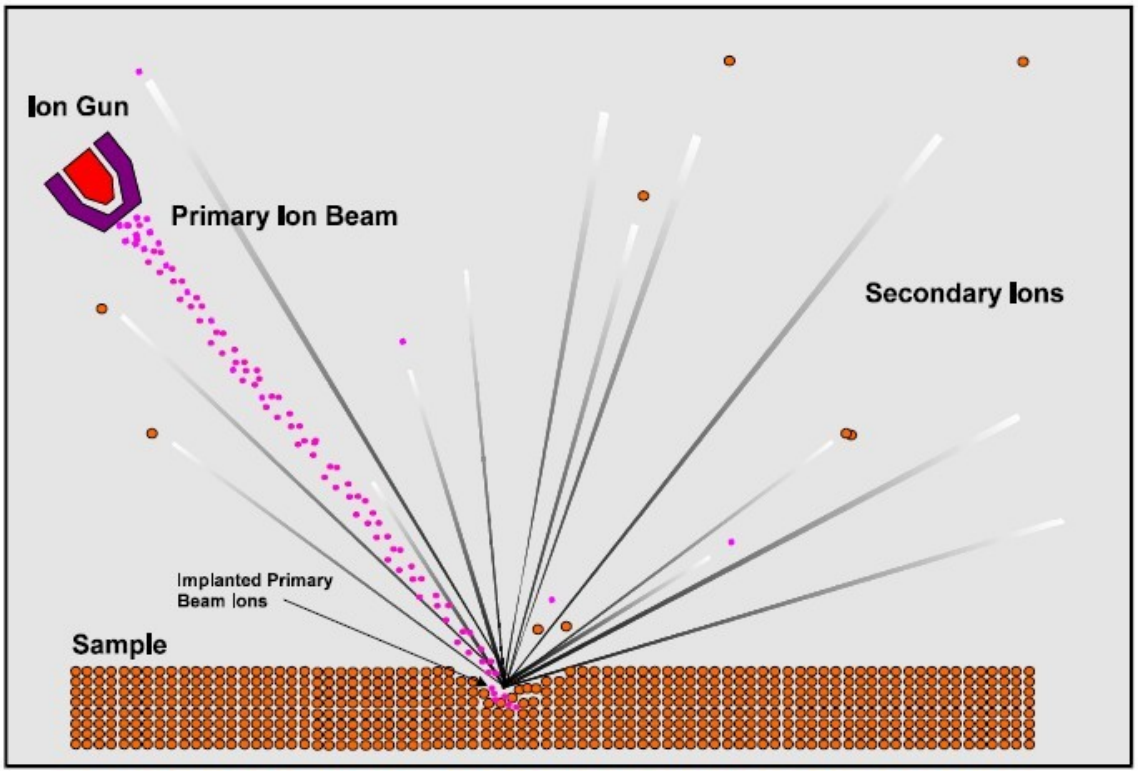

Figure 11. Diagram shows a sample being sputtered by a high energy beam of primary ions and ejected secondary ions.

sophisticated and sensitive mass spectrometers. The elements from H to U may be detected, most of which with concentrations down to 1 ppm or 1ppb. Isotopic ratios measured by SIMS may have a precision of 0.5% to 0.05%.

The SIMS instrument most common in geoscience is the ion microprobe, which uses a focused primary ion beam to sample target areas usually 10-μm to 50-μm diameter. The analysis for most samples is essentially non-destructive because the total sampling depth is typically less than 5 μm and the sampled mass only a few nanograms. Combined with surface imaging techniques such as backscattered electron (BSE) and cathodoluminescence (CL), SIMS can finely target the areas on a crystal surface (Ireland and Williams, 2003).

Zircon is particularly suitable for SIMS U-Th geochronology. Zircon ($ZrSiO_4$) is a common accessory mineral in igneous rocks, which can incorporate a series of trace elements including U and Th during its crystallization in the magma. The physical and chemical durability of zircon enables it to retain substantial chemical and isotopic information, providing insights into the evolution of Earth's crust and mantle (Finch and Hanchar, 2003). Zircons incorporate preferentially U relative to Th into the zircon lattice, resulting in significantly high $^{238}U/^{232}Th$ ratios in zircons. The subsequent increment in $^{230}Th/\ ^{238}U$ result from the decay of ^{238}U provides a means of determining the time that has elapsed since crystallization occurred. Furthermore, slow diffusion of U and Th in zircon results in preservation of U-Th crystallization ages (Reid et al., 1997). All these features make zircon crystals a highly effective U-Th dating tool.

PREVIOUS WORK

Li et al. (2000) performed the systematic K-Ar dating for Pliocene-Holocene volcanic eruptions, especially the latest eruptions of Heikongshan, Dayingshan, and Maanshan. They divided the activities of the Tengchong volcano into three stages: (1) those in southeastern and northwestern ends of the Tengchong volcanic area during late Pliocene; (2) during early Pleistocene, volcanism migrated and transferred to the central areas of the basin, of which the scale and distribution were the largest compared with the other stages; and (3) during the interval between early Pleistocene and Holocene, the volcanic scale decreased, and mainly distributed on a north-south-trending belt in the center of the Tengchong basin (early Pleistocene-middle Pleistocene). Young volcanic activity was clearly concentrated on Heikongshan, Dayingshan, and Maanshan. They also pointed out that, from the central north to south, the volcanic activity became progressively younger, which may indicate that the volcanism migrated from north to south.

Zhao and Fan (2010) analyzed the major elements, trace elements and strontium, neodymium and lead isotopic compositions of Maanshan, Dayingshan and Heikongshan volcanic rocks. Their Sr-Nd-Pb isotope data indicated that the Tengchong volcanoes originated from partial melting of a mixture of mid-ocean ridge basalts (MORB) and

enriched mantle. To explain why volcanic rocks in this intra-plate setting have the geochemical characteristics of island arcs or active continental margins, they proposed that the Neotethys oceanic crust was subducted beneath the Tengchong block and melted to produce the Tengchong volcanoes.

Chen et al. (2002) analyzed Nd-Sr-Pb isotopic compositions of Cenozoic volcanic rocks from Tengchong to explore their petrogenesis. They also collected country rock samples that,included amphibolites and Mesozoic to Cenozoic granitoids and measured their Nd-Sr-Pb isotopic compositions in order to evaluate the role of contamination and assimilation of country rocks during the formation of the volcanic rocks. They proposed that the origin of the Tengchong Cenozoic volcanic rocks is from partial melting of an enriched-mantle source, which probably resulted from assimilation of subducted slabs of the oceanic crust and sediments of the Neo-Tethyan basin. Crustal contamination during magma ascent is not significant.

Zou et al. (2010) used both conventional in-situ U-Th dating of polished zircon grains and U-Th depth profiling of unpolished grains to obtain zircon crystallization ages of the Maanshan Volcano, one of the youngest volcanoes in the Tengchong volcanic field. They concluded that the Maanshan zircons have two age populations at 91 ± 6 ka and 55 ± 7 ka. The 91 ka population represents zircon antecrysts derived from an earlier phase of andesitic magmatism, and the 55 ka population represents zircon phenocrysts that grew in the magma body itself before the eruption. Zou et al. (2010) also pointed out that Maanshan whole rocks have negative ε_{Nd} (-7.0) and high $^{87}Sr/^{86}Sr$ (0.7076), suggesting the source of Maanshan volcanic rocks may be an enriched mantle produced by continental subduction.

METHODS

Sample Preparation

Zircon crystals from Heikongshan volcanic rocks were isolated using standard mineral separation techniques, including magnetic methods and heavy liquids.

In a one-inch diameter aluminum disk, five 0.4 cm diameter holes are drilled and filled with soft indium metal. Individual zircon crystals are pressed into the indium metal in the mount (Fig. 12A). Instead of traditional epoxy, indium metal is used to avoid potential mass interferences of $^{230}Th_2{}^{12}C^{16}O^{2+}$ from epoxy on ^{230}Th isotopes. Figure 13 shows final mount of Heikongshan zircons after pressing into indium metal.

In order to produce a flat analysis surface of SIMS mounts, the mount should be polished by using the grinding paper. Another objective of polishing is to expose the interiors of zircon grains in the mount. Excessive polishing should be avoided, because this will tend to round grains in the mount and excavate trenches around them. The mount is then ultrasonically cleaned with soapy water and rinsed with deionized water. After the cleaning processes, the mount is placed in a drying oven at 50-75°C for at least one hour.

Before SIMS measurement, the mount must be coated with gold served as electrically conductive surface to make contact with the lip on the sample holder using the gold coater (Fig. 14). For most work in the geological sciences, gold and carbon are employed in the sample coating. In this study, gold coating is preferred because it is more

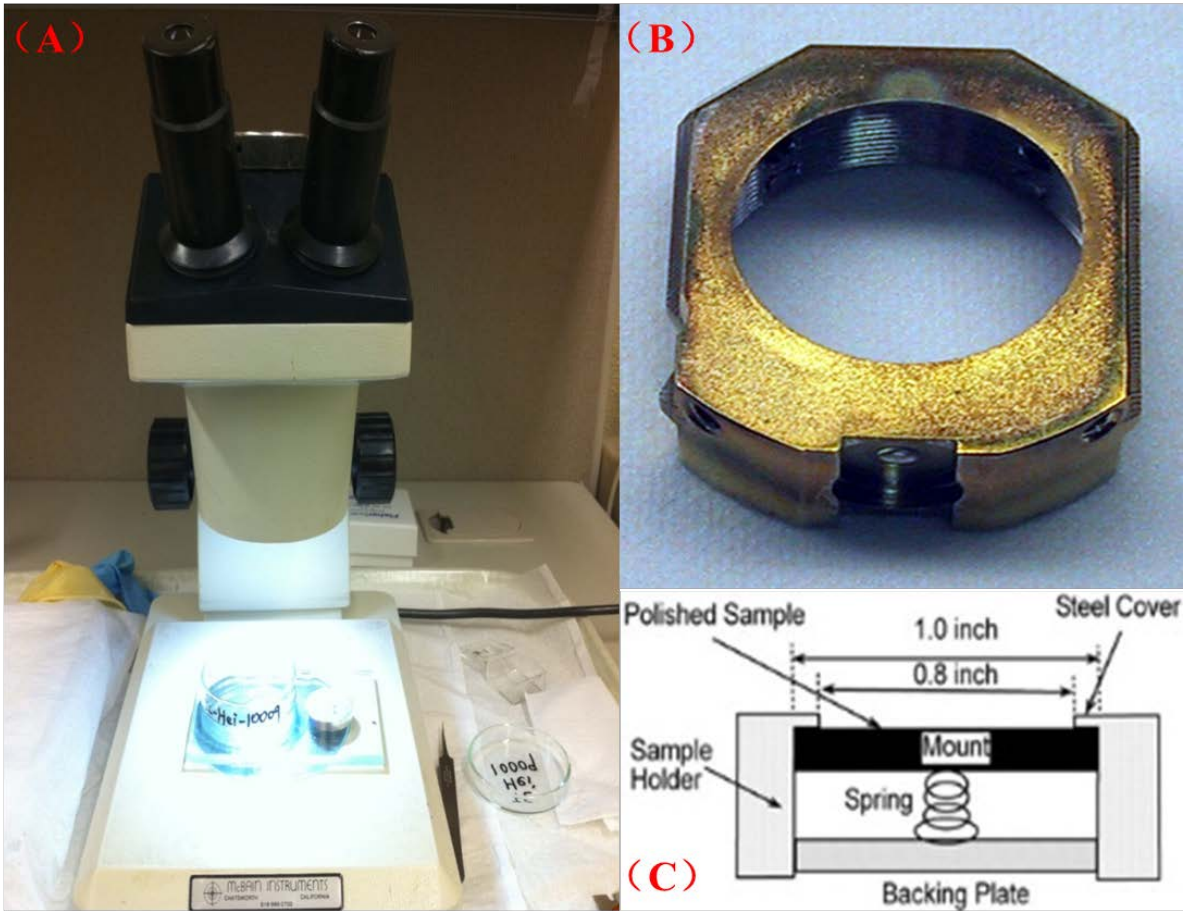

Figure 12. (A) Photograph of pressing zircons into the mount. (B) Photograph of a standard sample holder. (C) Schematic diagram of a sample holder showing backing plates and springs (From UCLA, 2010).

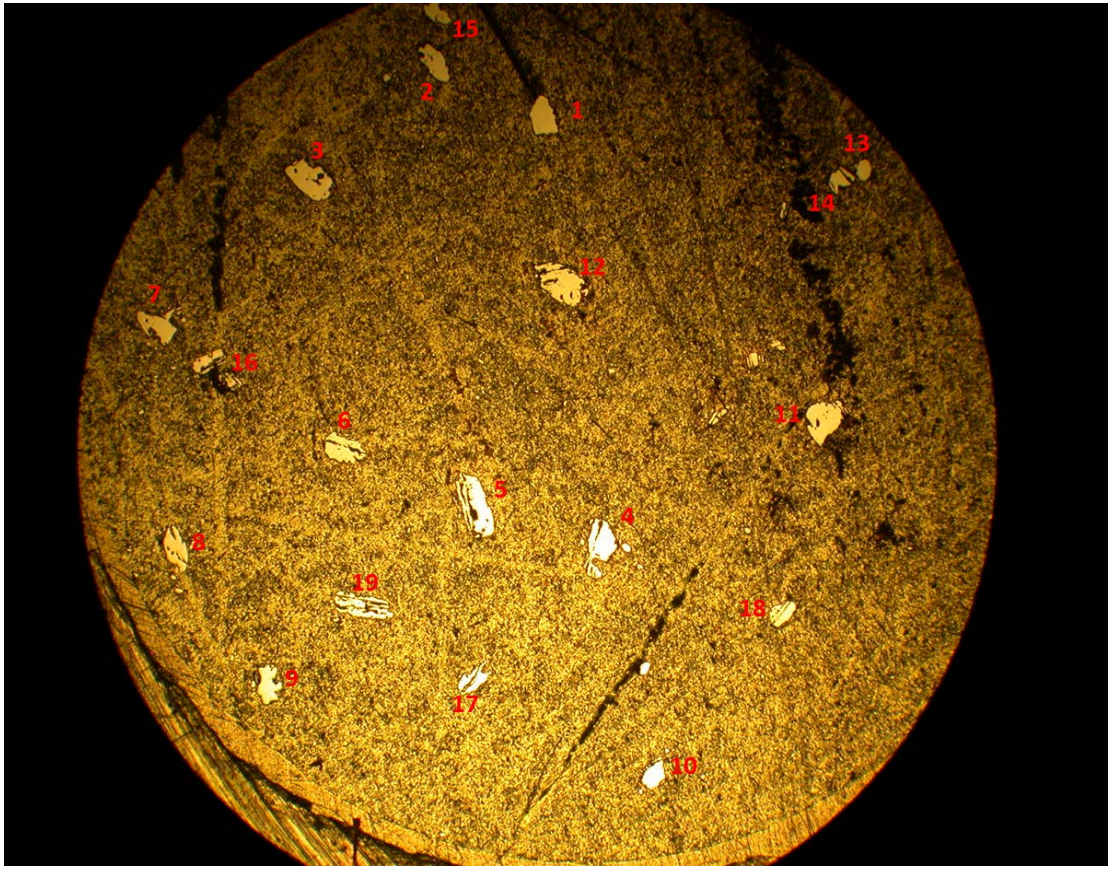

Figure 13. Final ring of Heikongshan zircons after pressing them into indium metal. Sample numbers are indicated in this figure. Note that the diameter of the ring is 0.4 cm.

Figure 14. Photograph of Gold Coater at the NSF National Ion Microprobe Facility at the University of California, Los Angeles (UCLA). The Gold Coater is used to coat a mount with gold served as electrically conductive surface to make contact with the lip on the sample holder.

conductive and more easily sputtered than carbon. In addition, mounts prepared for U-Th dating should avoid using carbon coating because of an isobaric interference of the small $^{230}Th^{16}O^{+}$ peak.

The Au-coated mount is placed in a sample holder (Fig. 13B and Fig. 13C), which are designed to accept 1-inch diameter cylindrical samples with a maximum thickness of about 1/2 cm. The sample mount is held against a machined lip by nonmagnetic spring and backing plate. The sample holder is then inserted into the CAMECA ims 1270 through an airlock system and then the sample is ready to be analyzed.

CAMECA ims 1270 Analytical Methods

$^{230}Th/^{232}Th$ and $^{238}U/^{232}Th$ atomic ratios of individual zircon crystals were measured using the CAMECA ims 1270 secondary ion mass spectrometer (SIMS) at UCLA (Figs. 15 and 16). Figure 16 shows a 3D schematic of the CAMECA ims 1270. Ion microprobe analyses of $^{230}Th/^{232}Th$ and $^{238}U/^{232}Th$ achieve a relative precision and accuracy of ~1-2% with a spot size of ~25 μm diameter (Zou et al., 2010). For the ion microprobe measurement, $^{16}O^{-}$ primary ion beam currents of 35-45 nA were focused on Au-coated zircons in the mount. Analyses were performed using a $^{16}O^{-}$ primary ion beam rather than O_2^{-} because experiment with $^{16}O^{-}$ primary beam yield higher intensity of stable secondary ion beams (Reid et al., 1997). As secondary ion yields higher intensity of oxides ($^{230}Th^{16}O^{+}$, $^{232}Th^{16}O^{+}$, and $^{238}U^{16}O^{+}$) than metals (e.g., $^{230}Th^{+}$), the oxide ions were measured to determine Th/U ratios.

Since ThO^{+} and UO^{+} have different ionization yields during sputtering, a correction factor should be applied to measured $^{230}Th^{16}O^{+}/^{238}U^{16}O^{+}$ and

Figure 15. Photograph of the CAMECA ims 1270 at the NSF National Ion Microprobe Facility at the University of California, Los Angeles (UCLA). (A) Lab plaque; (B) Sample chamber area; (C) User operating area.

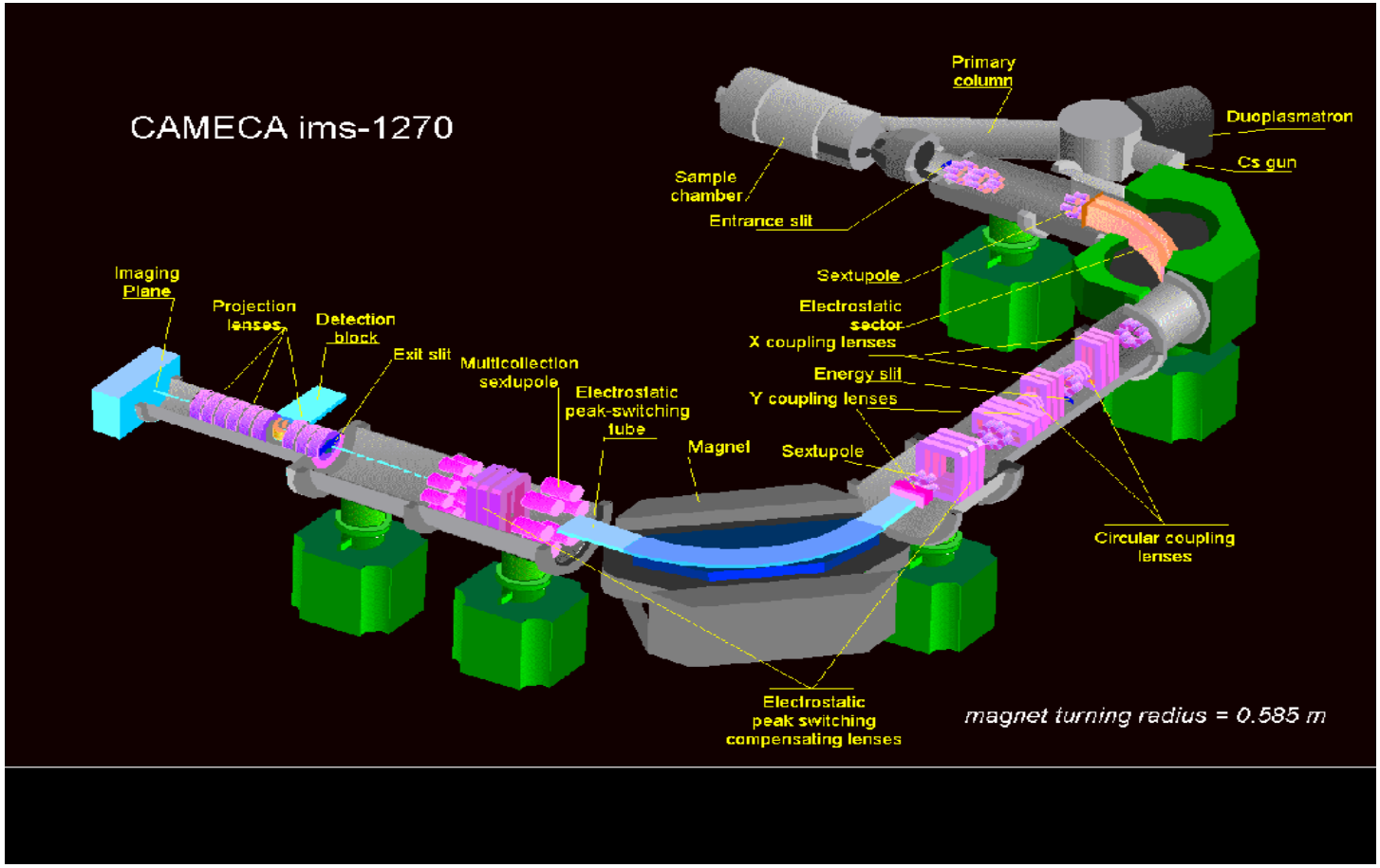

Figure 16. Cutaway schematic of the CAMECA ims 1270 ion microprobe in single collector mode (From UCLA, 2011).

$^{232}Th^{16}O^{+}/^{238}U^{16}O^{+}$ (Reid et al., 1997). The ThO^{+}/UO^{+} relative sensitivity factor (RSF) can be obtained by measuring the radiogenic $^{208}Pb/^{206}Pb$ ratio of old, concordant reference zircons AS-3 from Duluth Complex (Paces and Miller, 1993; Wiedenbeck et al., 1995). The zircon standard AS-3 has precisely known crystallization age of 1099.1± 0.7 Ga (Fig. 17) (Schmitz et al., 2001). Radiogenic $^{208}Pb/^{206}Pb$ is strongly correlated with measured $^{232}Th^{16}O^{+}/^{238}U^{16}O^{+}$ by the following relationship (Zou et al., 2010):

$$\frac{^{208}Pb_{std}}{^{206}Pb_{std}} = \frac{^{232}Th_{std}}{^{238}U_{std}} \times \frac{e^{\lambda_{232Th}t}-1}{e^{\lambda_{238U}t}-1} = 0.30062\frac{^{232}Th_{std}}{^{238}U_{std}}.$$

Th/U relative sensitivity factor can be calculated from standard AS-3 is

$$RSF = \frac{U^{+}_{std}}{^{238}U_{std}} / \frac{Th^{+}_{std}}{^{232}Th_{std}} = \frac{U^{+}_{std}}{Th^{+}_{std}} \times \frac{^{232}Th_{std}}{^{238}U_{std}} = \frac{U^{+}_{std}}{Th^{+}_{std}} \times \left(\frac{^{208}Pb_{std}/^{206}Pb_{std}}{0.30062}\right) = 3.3265\frac{^{208}Pb^{+}_{std}}{^{206}Pb^{+}_{std}} / \frac{UO^{+}_{std}}{ThO^{+}_{std}}.$$

Th/U relative sensitivity factors are 1.111 ± 0.020. The reference zircons are intermittently analyzed along with the unknowns during the analytical process. The mean square of the weighted deviation (MSWD) (Wendt and Carl, 1991) for these AS-3 standard data is 0.991 ± 0.010. The raw data for measured Heikongshan zircons are obtained and presented in Table 1.

Major and Trace Element Analyses

Whole-rock major and trace element concentrations of Heikongshan volcanic rocks were measured using X-ray fluorescence (XRF) and inductively coupled plasma

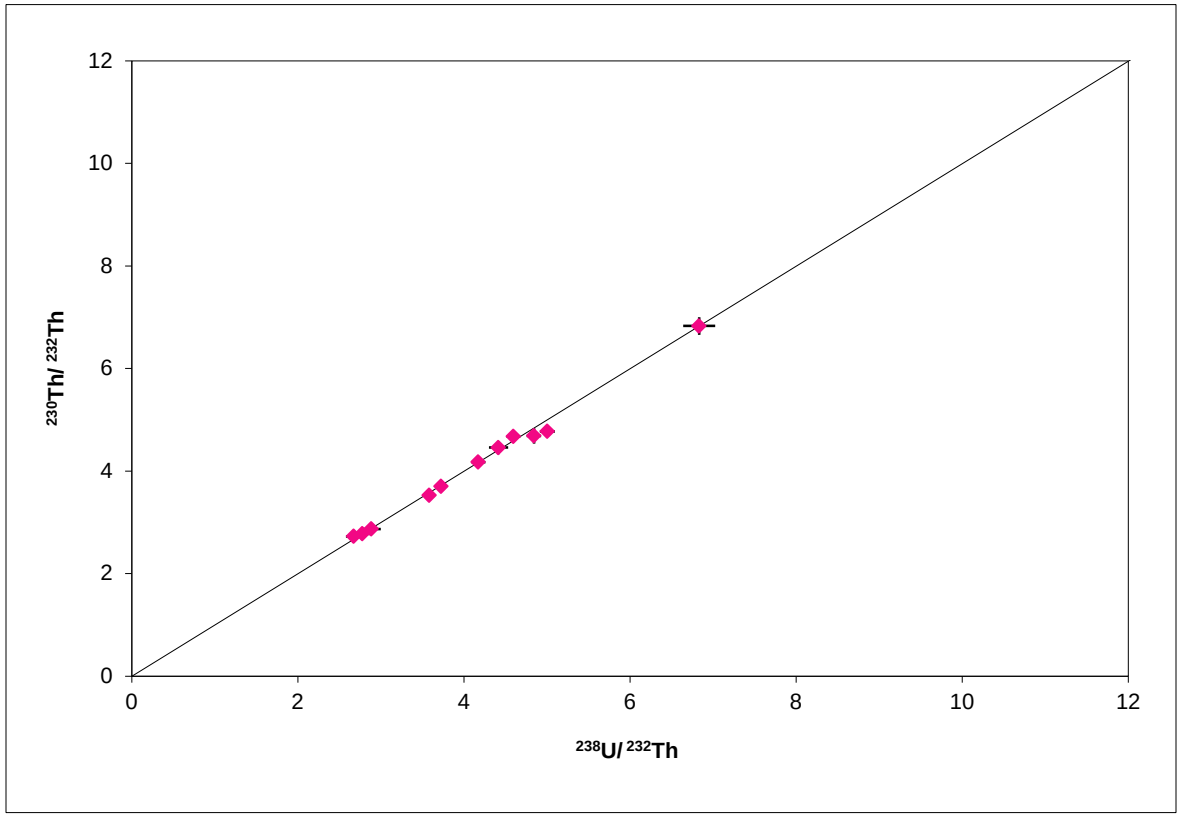

Figure 17. Plot of zircon standards AS-3 on the (^{230}Th/^{232}Th) vs. (^{238}U/^{232}Th) diagram. Note that all zircon standard AS-3 plot on the equiline. Note that some error bars are smaller than symbols.

Table 1

Raw data for Heikongshan zircon crystals collected from SIMS analyses. 1 s.e. is the standard error, which represents measurement uncertainty.

Sample	*246.02804/ U O*	*246.02804/ U O*	*U O/ Th O*	*U O/ Th O*	*246.02804/ Th O*	*246.02804/ Th O*
		1 s.e.		*1 s.e.*		*1 s.e.*
2011_08_20Aug\ Hei@1.ais	1.08E-05	2.42E-07	6.27E-01	2.29E-03	6.81E-06	1.61E-07
2011_08_20Aug\ Hei@2.ais	1.16E-05	3.38E-07	4.54E-01	4.87E-04	5.28E-06	1.53E-07
2011_08_20Aug\ Hei@3.ais	1.17E-05	3.06E-07	5.48E-01	3.22E-04	6.43E-06	1.68E-07
2011_08_20Aug\ Hei@4.ais	1.10E-05	2.23E-07	4.71E-01	7.58E-04	5.17E-06	1.05E-07
2011_08_20Aug\ Hei@5.ais	1.13E-05	5.31E-07	3.45E-01	3.11E-03	3.90E-06	1.89E-07
2011_08_20Aug\ Hei@7.ais	1.09E-05	3.12E-07	7.04E-01	1.21E-03	7.64E-06	2.20E-07
2011_08_20Aug\ Hei@8.ais	1.12E-05	2.49E-07	4.55E-01	2.81E-03	5.12E-06	1.25E-07
2011_08_20Aug\ Hei@9.ais	1.10E-05	4.23E-07	3.83E-01	4.50E-04	4.23E-06	1.62E-07
2011_08_20Aug\ Hei@11.ais	1.11E-05	5.87E-07	7.91E-01	1.38E-03	8.77E-06	4.65E-07
2011_08_20Aug\ Hei@12.ais	1.20E-05	3.60E-07	5.21E-01	2.18E-03	6.22E-06	1.90E-07
2011_08_20Aug\ Hei@13.ais	1.09E-05	4.55E-07	3.96E-01	3.07E-03	4.31E-06	1.80E-07
2011_08_20Aug\ Hei@14.ais	1.62E-05	5.81E-07	3.10E-01	2.10E-03	5.04E-06	2.03E-07
2011_08_20Aug\ Hei@15.ais	1.00E-05	2.33E-07	9.58E-01	3.34E-02	9.57E-06	3.73E-07
2011_08_20Aug\ Hei@16.ais	1.12E-05	2.82E-07	6.81E-01	6.65E-03	7.65E-06	2.50E-07
2011_08_20Aug\ Hei@17.ais	1.11E-05	4.62E-07	6.96E-01	6.72E-04	7.73E-06	3.23E-07
2011_08_20Aug\ Hei@18.ais	1.37E-05	9.43E-07	5.54E-01	5.95E-03	7.49E-06	5.17E-07
2011_08_20Aug\ Hei@19.ais	1.32E-05	4.51E-07	1.89E-01	5.43E-04	2.49E-06	8.74E-08
2011_08_20Aug\ Hei@3sp2.ais	1.15E-05	2.06E-07	5.81E-01	2.44E-03	6.65E-06	1.19E-07
2011_08_20Aug\ Hei@4sp2.ais	1.12E-05	2.68E-07	6.36E-01	1.04E-03	7.13E-06	1.75E-07
2011_08_20Aug\ Hei@5sp2.ais	1.18E-05	5.50E-07	3.23E-01	8.00E-03	3.81E-06	2.31E-07
2011_08_20Aug\ Hei@8sp2.ais	1.12E-05	2.24E-07	4.80E-01	3.51E-04	5.38E-06	1.07E-07
2011_08_20Aug\ Hei@9sp2.ais	1.12E-05	4.63E-07	4.54E-01	4.95E-03	5.10E-06	2.25E-07
2011_08_20Aug\ Hei@11sp2.ais	1.08E-05	2.80E-07	1.10E+00	2.67E-02	1.21E-05	3.71E-07
2011_08_20Aug\ Hei@12sp2.ais	1.18E-05	4.06E-07	4.55E-01	1.52E-03	5.37E-06	1.77E-07

Table 1 continued

Raw data for Heikongshan zircon crystals collected from SIMS analyses. 1 s.e. is the standard error, which represents measurement uncertainty.

Sample	*246.3/*	*246.3/*	*246.3/*	*246.3/*	*244.0381/*	*244.0381/*
	U O	*U O*	*Th O*	*Th O*	*U O*	*U O*
		1 s.e.		*1 s.e.*		*1 s.e.*
2011_08_20Aug\ Hei@1.ais	1.95E-07	7.48E-08	1.21E-07	4.67E-08	3.25E-07	6.38E-08
2011_08_20Aug\ Hei@2.ais	1.99E-07	9.83E-08	9.07E-08	4.47E-08	5.11E-07	1.24E-07
2011_08_20Aug\ Hei@3.ais	5.19E-08	3.40E-08	2.85E-08	1.86E-08	2.11E-07	5.34E-08
2011_08_20Aug\ Hei@4.ais	1.47E-07	6.38E-08	6.89E-08	2.98E-08	2.84E-07	6.79E-08
2011_08_20Aug\ Hei@5.ais	5.19E-07	2.25E-07	1.82E-07	7.81E-08	1.60E-06	3.43E-07
2011_08_20Aug\ Hei@7.ais	2.43E-07	8.22E-08	1.72E-07	5.82E-08	4.32E-07	1.01E-07
2011_08_20Aug\ Hei@8.ais	2.41E-07	7.52E-08	1.10E-07	3.43E-08	4.86E-07	8.54E-08
2011_08_20Aug\ Hei@9.ais	2.80E-07	1.93E-07	1.08E-07	7.39E-08	8.90E-07	2.26E-07
2011_08_20Aug\ Hei@11.ais	4.92E-07	2.37E-07	3.91E-07	1.88E-07	1.07E-06	2.59E-07
2011_08_20Aug\ Hei@12.ais	2.49E-07	1.08E-07	1.32E-07	5.73E-08	5.16E-07	1.24E-07
2011_08_20Aug\ Hei@13.ais	2.47E-07	1.83E-07	9.55E-08	7.07E-08	1.20E-06	2.78E-07
2011_08_20Aug\ Hei@14.ais	5.37E-07	2.66E-07	1.68E-07	8.36E-08	8.96E-06	9.55E-07
2011_08_20Aug\ Hei@15.ais	1.28E-07	6.63E-08	1.19E-07	6.01E-08	2.65E-07	7.17E-08
2011_08_20Aug\ Hei@16.ais	2.08E-07	7.70E-08	1.43E-07	5.37E-08	3.62E-06	3.59E-07
2011_08_20Aug\ Hei@17.ais	4.22E-07	1.86E-07	2.94E-07	1.29E-07	2.07E-06	3.31E-07
2011_08_20Aug\ Hei@18.ais	1.70E-06	7.31E-07	9.62E-07	4.12E-07	5.12E-06	1.04E-06
2011_08_20Aug\ Hei@19.ais	2.03E-07	1.36E-07	3.88E-08	2.58E-08	9.12E-07	1.91E-07
2011_08_20Aug\ Hei@3sp2.ais	1.61E-07	5.32E-08	9.18E-08	3.05E-08	2.20E-07	5.49E-08
2011_08_20Aug\ Hei@4sp2.ais	7.08E-08	4.32E-08	4.53E-08	2.76E-08	1.38E-06	2.12E-07
2011_08_20Aug\ Hei@5sp2.ais	3.01E-07	1.72E-07	1.13E-07	6.70E-08	1.16E-06	2.29E-07
2011_08_20Aug\ Hei@8sp2.ais	1.68E-07	5.34E-08	8.08E-08	2.56E-08	2.37E-07	5.79E-08
2011_08_20Aug\ Hei@9sp2.ais	4.79E-07	2.02E-07	2.11E-07	8.90E-08	3.97E-07	1.59E-07
2011_08_20Aug\ Hei@11sp2.ais	2.06E-07	9.65E-08	2.21E-07	1.06E-07	5.74E-07	1.16E-07
2011_08_20Aug\ Hei@12sp2.ais	4.16E-07	1.62E-07	1.90E-07	7.41E-08	1.04E-06	2.01E-07

Table 1 continued

Raw data for Heikongshan zircon crystals collected from SIMS analyses. 1 s.e. is the standard error, which represents measurement uncertainty.

Sample	*244.0381/*	*244.0381/*	*U O/*	*U O/*	*246.3*	*92Zr Zr O4*
	Th O	*Th O*	*Zr2 O4*	*Zr2 O4*		
		1 s.e.		*1 s.e.*		
2011_08_20Aug\ Hei@1.ais	2.04E-07	4.00E-08	1.44E+01	1.10E-01	0.1212	2.99E+04
2011_08_20Aug\ Hei@2.ais	2.32E-07	5.62E-08	5.87E+00	4.04E-02	0.05092	3.03E+04
2011_08_20Aug\ Hei@3.ais	1.16E-07	2.93E-08	2.20E+01	3.60E-01	0.04762	2.77E+04
2011_08_20Aug\ Hei@4.ais	1.33E-07	3.19E-08	1.23E+01	1.25E-01	0.07586	2.91E+04
2011_08_20Aug\ Hei@5.ais	5.43E-07	1.17E-07	2.98E+00	3.04E-02	0.06063	2.57E+04
2011_08_20Aug\ Hei@7.ais	3.04E-07	7.11E-08	7.94E+00	1.71E-02	0.08333	2.99E+04
2011_08_20Aug\ Hei@8.ais	2.24E-07	3.94E-08	1.37E+01	3.26E-01	0.1287	3.16E+04
2011_08_20Aug\ Hei@9.ais	3.42E-07	8.66E-08	3.46E+00	3.84E-02	0.03785	3.09E+04
2011_08_20Aug\ Hei@11.ais	8.44E-07	2.05E-07	2.79E+00	2.86E-02	0.06061	3.04E+04
2011_08_20Aug\ Hei@12.ais	2.71E-07	6.51E-08	6.21E+00	8.70E-02	0.06063	3.11E+04
2011_08_20Aug\ Hei@13.ais	4.71E-07	1.09E-07	3.00E+00	2.45E-02	0.03029	3.07E+04
2011_08_20Aug\ Hei@14.ais	2.84E-06	3.08E-07	4.03E+00	7.03E-02	0.0833	3.43E+04
2011_08_20Aug\ Hei@15.ais	2.35E-07	6.23E-08	2.12E+01	1.45E+00	0.1289	4.38E+04
2011_08_20Aug\ Hei@16.ais	2.54E-06	2.65E-07	1.03E+01	2.98E-01	0.09635	4.93E+04
2011_08_20Aug\ Hei@17.ais	1.44E-06	2.30E-07	4.11E+00	3.45E-02	0.06059	3.19E+04
2011_08_20Aug\ Hei@18.ais	2.88E-06	5.88E-07	7.92E-01	4.55E-03	0.06055	3.81E+04
2011_08_20Aug\ Hei@19.ais	1.73E-07	3.62E-08	7.87E+00	1.56E-01	0.05831	4.35E+04
2011_08_20Aug\ Hei@3sp2.ais	1.29E-07	3.22E-08	1.44E+01	2.50E-01	0.1138	3.05E+04
2011_08_20Aug\ Hei@4sp2.ais	8.75E-07	1.36E-07	1.01E+01	1.32E-01	0.03031	2.95E+04
2011_08_20Aug\ Hei@5sp2.ais	4.10E-07	9.14E-08	4.21E+00	2.88E-01	0.04335	4.31E+04
2011_08_20Aug\ Hei@8sp2.ais	1.14E-07	2.78E-08	1.60E+01	8.85E-02	0.09851	2.96E+04
2011_08_20Aug\ Hei@9sp2.ais	1.79E-07	7.16E-08	4.21E+00	3.80E-02	0.05514	2.25E+04
2011_08_20Aug\ Hei@11sp2.ais	6.86E-07	1.38E-07	7.56E+00	9.81E-02	0.06814	3.45E+04
2011_08_20Aug\ Hei@12sp2.ais	4.72E-07	9.13E-08	5.44E+00	3.84E-02	0.08329	2.80E+04

Table 1 continued

Raw data for Heikongshan zircon crystals collected from SIMS analyses. 1 s.e. is the standard error, which represents measurement uncertainty.

Sample	*246.02804*	*244.0381*	*Bckgr*			
			U O	*U O*	*Th O*	*Th O*
				1 s.e.		*1 s.e.*
2011_08_20Aug\ Hei@1.ais	6.449	1.97E-01	2.60E-07	6.95279E-08	1.63E-07	4.34616E-08
2011_08_20Aug\ Hei@2.ais	2.874	1.29E-01	3.55E-07	1.11775E-07	1.61E-07	5.07856E-08
2011_08_20Aug\ Hei@3.ais	9.99	1.85E-01	1.31E-07	4.47462E-08	7.20E-08	2.45457E-08
2011_08_20Aug\ Hei@4.ais	5.517	1.32E-01	2.15E-07	6.58977E-08	1.01E-07	3.08624E-08
2011_08_20Aug\ Hei@5.ais	1.221	1.65E-01	1.06E-06	2.903E-07	3.63E-07	9.91723E-08
2011_08_20Aug\ Hei@7.ais	3.577	1.39E-01	3.37E-07	9.21404E-08	2.38E-07	6.49376E-08
2011_08_20Aug\ Hei@8.ais	6.166	2.46E-01	3.64E-07	8.04272E-08	1.67E-07	3.69307E-08
2011_08_20Aug\ Hei@9.ais	1.552	1.18E-01	5.85E-07	2.0965E-07	2.25E-07	8.05124E-08
2011_08_20Aug\ Hei@11.ais	1.313	1.29E-01	7.79E-07	2.4794E-07	6.17E-07	1.96523E-07
2011_08_20Aug\ Hei@12.ais	3.245	1.31E-01	3.82E-07	1.16276E-07	2.01E-07	6.13441E-08
2011_08_20Aug\ Hei@13.ais	1.309	1.42E-01	7.25E-07	2.35186E-07	2.83E-07	9.18242E-08
2011_08_20Aug\ Hei@14.ais	2.505	1.28E+00	4.75E-06	7.01265E-07	1.50E-06	2.25604E-07
2011_08_20Aug\ Hei@15.ais	9.377	1.97E-01	1.97E-07	6.90724E-08	1.77E-07	6.12204E-08
2011_08_20Aug\ Hei@16.ais	5.201	1.50E+00	1.91E-06	2.59354E-07	1.34E-06	1.9098E-07
2011_08_20Aug\ Hei@17.ais	1.626	2.95E-01	1.24E-06	2.68413E-07	8.65E-07	1.86511E-07
2011_08_20Aug\ Hei@18.ais	0.4772	1.82E-01	3.41E-06	9.01355E-07	1.92E-06	5.07922E-07
2011_08_20Aug\ Hei@19.ais	4.158	2.81E-01	5.58E-07	1.65986E-07	1.06E-07	3.14397E-08
2011_08_20Aug\ Hei@3sp2.ais	7.066	1.21E-01	1.90E-07	5.40816E-08	1.10E-07	3.13669E-08
2011_08_20Aug\ Hei@4sp2.ais	4.277	4.75E-01	7.23E-07	1.53126E-07	4.60E-07	9.79147E-08
2011_08_20Aug\ Hei@5sp2.ais	2.549	2.02E-01	7.32E-07	2.02614E-07	2.61E-07	8.01695E-08
2011_08_20Aug\ Hei@8sp2.ais	6.665	1.27E-01	2.02E-07	5.57043E-08	9.71E-08	2.67166E-08
2011_08_20Aug\ Hei@9sp2.ais	1.345	4.76E-02	4.38E-07	1.81323E-07	1.95E-07	8.07909E-08
2011_08_20Aug\ Hei@11sp2.ais	3.562	1.87E-01	3.90E-07	1.0642E-07	4.53E-07	1.22859E-07
2011_08_20Aug\ Hei@12sp2.ais	2.306	2.02E-01	7.27E-07	1.82534E-07	3.31E-07	8.31261E-08

Table 1 continued

Raw data for Heikongshan zircon crystals collected from SIMS analyses. 1 s.e. is the standard error, which represents measurement uncertainty.

	(246.3 only)					
Sample	**246.029/ U O**	**246.029/ U O 1 s.e.**	**U O/ Th O**	**U O/ Th O 1 s.e.**	**246.029/ Th O**	**246.029/ Th O 1 s.e.**
2011_08_20Aug\ Hei@1.ais	1.06453E-05	2.53E-07	0.6273	2.29E-03	6.6869E-06	1.68E-07
2011_08_20Aug\ Hei@2.ais	1.14406E-05	3.52E-07	0.4537	4.87E-04	5.19127E-06	1.59E-07
2011_08_20Aug\ Hei@3.ais	1.16781E-05	3.07E-07	0.5482	3.22E-04	6.40554E-06	1.69E-07
2011_08_20Aug\ Hei@4.ais	0.000010843	2.32E-07	0.4706	7.58E-04	5.10413E-06	1.09E-07
2011_08_20Aug\ Hei@5.ais	0.000010751	5.77E-07	0.3453	3.11E-03	3.7176E-06	2.05E-07
2011_08_20Aug\ Hei@7.ais	1.06173E-05	3.22E-07	0.7035	1.21E-03	7.4683E-06	2.27E-07
2011_08_20Aug\ Hei@8.ais	1.09888E-05	2.60E-07	0.4551	2.81E-03	5.0048E-06	1.30E-07
2011_08_20Aug\ Hei@9.ais	0.00001076	4.64E-07	0.3834	4.50E-04	4.1255E-06	1.78E-07
2011_08_20Aug\ Hei@11.ais	1.05982E-05	6.33E-07	0.791	1.38E-03	8.3812E-06	5.01E-07
2011_08_20Aug\ Hei@12.ais	1.17009E-05	3.76E-07	0.5206	2.18E-03	6.0904E-06	1.98E-07
2011_08_20Aug\ Hei@13.ais	1.06629E-05	4.90E-07	0.3963	3.07E-03	4.21152E-06	1.93E-07
2011_08_20Aug\ Hei@14.ais	1.56433E-05	6.39E-07	0.3096	2.10E-03	4.8711E-06	2.19E-07
2011_08_20Aug\ Hei@15.ais	9.8817E-06	2.42E-07	0.9577	3.34E-02	9.4477E-06	3.78E-07
2011_08_20Aug\ Hei@16.ais	1.09617E-05	2.92E-07	0.6806	6.65E-03	7.5074E-06	2.56E-07
2011_08_20Aug\ Hei@17.ais	1.06878E-05	4.98E-07	0.6956	6.72E-04	7.4398E-06	3.48E-07
2011_08_20Aug\ Hei@18.ais	0.000011961	1.19E-06	0.5542	5.95E-03	6.5291E-06	6.61E-07
2011_08_20Aug\ Hei@19.ais	1.29666E-05	4.71E-07	0.1889	5.43E-04	2.45018E-06	9.12E-08
2011_08_20Aug\ Hei@3sp2.ais	1.12992E-05	2.12E-07	0.5808	2.44E-03	6.56122E-06	1.23E-07
2011_08_20Aug\ Hei@4sp2.ais	1.11492E-05	2.71E-07	0.6355	1.04E-03	7.08873E-06	1.77E-07
2011_08_20Aug\ Hei@5sp2.ais	1.14587E-05	5.77E-07	0.3226	8.00E-03	3.6934E-06	2.41E-07
2011_08_20Aug\ Hei@8sp2.ais	1.10318E-05	2.30E-07	0.4803	3.51E-04	5.29825E-06	1.10E-07
2011_08_20Aug\ Hei@9sp2.ais	1.07408E-05	5.05E-07	0.4538	4.95E-03	4.8871E-06	2.42E-07
2011_08_20Aug\ Hei@11sp2.ais	0.000010554	2.96E-07	1.097	2.67E-02	1.18291E-05	3.86E-07
2011_08_20Aug\ Hei@12sp2.ais	1.14044E-05	4.37E-07	0.4549	1.52E-03	5.1779E-06	1.92E-07

Table 1 continued

Raw data for Heikongshan zircon crystals collected from SIMS analyses. 1 s.e. is the standard error, which represents measurement uncertainty.

	(average 246.3 + 244.038)					
Sample	**246.029/**	**246.029/**	**U O/**	**U O/**	**246.029/**	**246.029/**
	U O	**U O**	**Th O**	**Th O**	**Th O**	**Th O**
		1 s.e.		**1 s.e.**		**1 s.e.**
2011_08_20Aug\ Hei@1.ais	1.06E-05	2.51694E-07	6.27E-01	0.002289	6.65E-06	1.66956E-07
2011_08_20Aug\ Hei@2.ais	1.13E-05	3.56097E-07	4.54E-01	0.0004865	5.12E-06	1.61208E-07
2011_08_20Aug\ Hei@3.ais	1.16E-05	3.0876E-07	5.48E-01	0.0003216	6.36E-06	1.69388E-07
2011_08_20Aug\ Hei@4.ais	1.08E-05	2.32629E-07	4.71E-01	0.0007575	5.07E-06	1.09442E-07
2011_08_20Aug\ Hei@5.ais	1.02E-05	6.05086E-07	3.45E-01	0.003111	3.54E-06	2.13705E-07
2011_08_20Aug\ Hei@7.ais	1.05E-05	3.25033E-07	7.04E-01	0.001209	7.40E-06	2.28904E-07
2011_08_20Aug\ Hei@8.ais	1.09E-05	2.61572E-07	4.55E-01	0.002811	4.95E-06	1.30629E-07
2011_08_20Aug\ Hei@9.ais	1.05E-05	4.71746E-07	3.83E-01	0.00045	4.01E-06	1.80904E-07
2011_08_20Aug\ Hei@11.ais	1.03E-05	6.37491E-07	7.91E-01	0.001382	8.15E-06	5.04639E-07
2011_08_20Aug\ Hei@12.ais	1.16E-05	3.78407E-07	5.21E-01	0.002176	6.02E-06	1.99277E-07
2011_08_20Aug\ Hei@13.ais	1.02E-05	5.11834E-07	3.96E-01	0.003066	4.02E-06	2.01623E-07
2011_08_20Aug\ Hei@14.ais	1.14E-05	9.10933E-07	3.10E-01	0.002096	3.54E-06	3.03357E-07
2011_08_20Aug\ Hei@15.ais	9.81E-06	2.42639E-07	9.58E-01	0.03336	9.39E-06	3.78089E-07
2011_08_20Aug\ Hei@16.ais	9.26E-06	3.82836E-07	6.81E-01	0.006649	6.31E-06	3.14521E-07
2011_08_20Aug\ Hei@17.ais	9.87E-06	5.34053E-07	6.96E-01	0.0006723	6.87E-06	3.73155E-07
2011_08_20Aug\ Hei@18.ais	1.03E-05	1.30427E-06	5.54E-01	0.005951	5.57E-06	7.24687E-07
2011_08_20Aug\ Hei@19.ais	1.26E-05	4.80575E-07	1.89E-01	0.0005425	2.38E-06	9.2911E-08
2011_08_20Aug\ Hei@3sp2.ais	1.13E-05	2.12497E-07	5.81E-01	0.002437	6.54E-06	1.23355E-07
2011_08_20Aug\ Hei@4sp2.ais	1.05E-05	3.084E-07	6.36E-01	0.001044	6.67E-06	2.00356E-07
2011_08_20Aug\ Hei@5sp2.ais	1.10E-05	5.86509E-07	3.23E-01	0.007999	3.54E-06	2.44894E-07
2011_08_20Aug\ Hei@8sp2.ais	1.10E-05	2.31016E-07	4.80E-01	0.0003512	5.28E-06	1.10285E-07
2011_08_20Aug\ Hei@9sp2.ais	1.08E-05	4.97612E-07	4.54E-01	0.004954	4.90E-06	2.39348E-07
2011_08_20Aug\ Hei@11sp2.ais	1.04E-05	2.99168E-07	1.10E+00	0.02671	1.16E-05	3.90814E-07
2011_08_20Aug\ Hei@12sp2.ais	1.11E-05	4.44781E-07	4.55E-01	0.001524	5.04E-06	1.95729E-07

Table 1 continued

Raw data for Heikongshan zircon crystals collected from SIMS analyses. 1 s.e. is the standard error, which represents measurement uncertainty.

	gain corrected(average gain 1.000E + 00)					
Sample	**246.029/**	**246.029/**	**U O/**	**U O/**	**246.029/**	**246.029/**
	U O	**U O**	**Th O**	**Th O**	**Th O**	**Th O**
		1 s.e.		**1 s.e.**		**1 s.e.**
2011_08_20Aug\ Hei@1.ais	1.06E-05	2.51694E-07	6.27E-01	0.002289	6.65E-06	1.66956E-07
2011_08_20Aug\ Hei@2.ais	1.13E-05	3.56097E-07	4.54E-01	0.0004865	5.12E-06	1.61208E-07
2011_08_20Aug\ Hei@3.ais	1.16E-05	3.0876E-07	5.48E-01	0.0003216	6.36E-06	1.69388E-07
2011_08_20Aug\ Hei@4.ais	1.08E-05	2.32629E-07	4.71E-01	0.0007575	5.07E-06	1.09442E-07
2011_08_20Aug\ Hei@5.ais	1.02E-05	6.05086E-07	3.45E-01	0.003111	3.54E-06	2.13705E-07
2011_08_20Aug\ Hei@7.ais	1.05E-05	3.25033E-07	7.04E-01	0.001209	7.40E-06	2.28904E-07
2011_08_20Aug\ Hei@8.ais	1.09E-05	2.61572E-07	4.55E-01	0.002811	4.95E-06	1.30629E-07
2011_08_20Aug\ Hei@9.ais	1.05E-05	4.71746E-07	3.83E-01	0.00045	4.01E-06	1.80904E-07
2011_08_20Aug\ Hei@11.ais	1.03E-05	6.37491E-07	7.91E-01	0.001382	8.15E-06	5.04639E-07
2011_08_20Aug\ Hei@12.ais	1.16E-05	3.78407E-07	5.21E-01	0.002176	6.02E-06	1.99277E-07
2011_08_20Aug\ Hei@13.ais	1.02E-05	5.11834E-07	3.96E-01	0.003066	4.02E-06	2.01623E-07
2011_08_20Aug\ Hei@14.ais	1.56E-05	6.39361E-07	3.10E-01	0.002096	4.87E-06	2.19363E-07
2011_08_20Aug\ Hei@15.ais	9.81E-06	2.42639E-07	9.58E-01	0.03336	9.39E-06	3.78089E-07
2011_08_20Aug\ Hei@16.ais	1.10E-05	2.91948E-07	6.81E-01	0.006649	7.51E-06	2.55598E-07
2011_08_20Aug\ Hei@17.ais	9.87E-06	5.34053E-07	6.96E-01	0.0006723	6.87E-06	3.73155E-07
2011_08_20Aug\ Hei@18.ais	1.03E-05	1.30427E-06	5.54E-01	0.005951	5.57E-06	7.24687E-07
2011_08_20Aug\ Hei@19.ais	1.26E-05	4.80575E-07	1.89E-01	0.0005425	2.38E-06	9.2911E-08
2011_08_20Aug\ Hei@3sp2.ais	1.13E-05	2.12497E-07	5.81E-01	0.002437	6.54E-06	1.23355E-07
2011_08_20Aug\ Hei@4sp2.ais	1.05E-05	3.084E-07	6.36E-01	0.001044	6.67E-06	2.00356E-07
2011_08_20Aug\ Hei@5sp2.ais	1.10E-05	5.86509E-07	3.23E-01	0.007999	3.54E-06	2.44894E-07
2011_08_20Aug\ Hei@8sp2.ais	1.10E-05	2.31016E-07	4.80E-01	0.0003512	5.28E-06	1.10285E-07
2011_08_20Aug\ Hei@9sp2.ais	1.08E-05	4.97612E-07	4.54E-01	0.004954	4.90E-06	2.39348E-07
2011_08_20Aug\ Hei@11sp2.ais	1.04E-05	2.99168E-07	1.10E+00	0.02671	1.16E-05	3.90814E-07
2011_08_20Aug\ Hei@12sp2.ais	1.11E-05	4.44781E-07	4.55E-01	0.001524	5.04E-06	1.95729E-07

mass spectrometry (ICP-MS), respectively, by the GeoAnalytical Lab, School of Earth and Environmental Sciences, Washington State University. Relative errors for major elements are SiO_2 (0.4%), TiO_2 (0.4%), Al_2O_3 (0.4%), FeO (0.6%), MnO (1%), MgO (0.5%), CaO (0.2%), Na_2O (0.9%), K_2O (0.4%), and P_2O_5 (2%). Relative errors for most trace element analyses are estimated to be < 4%, except for Ta (6%), Cs (6%), Pb (7%), Sc (7%), Th (16%), and U (16%).

Results

Whole-Rock Major and Trace Element Analysis

The major and trace element concentrations of sample Hei-10009 from Heikongshan are presented in Table 2. The rock type of Hei-10009 is basaltic trachyandesite (Fig. 18) and is potassium rich. Sample Hei-10009 has SiO_2 content of 54%, which is lower than Maanshan (56.91%-59.34%) (Wang et al., 2006; Zou et al., 2010) and Dayingshan (61%-62.17%) (Wang et al., 2006; Tucker, 2011). Generally, the major and trace element concentrations of Hei-10009 yielded similar results from previous data from the Heikongshan Holocene volcanic rocks. These major element concentrations, along with those from other rocks collected from Maanshan and Dayingshan (Wang et al., 2006; Zou et al., 2010; Zhao et al., 2010) (Table 3) were plotted on conventional Harker diagram (Figs. 19 and 20). The data show clear variations in these elements with a considerable range in SiO_2 content.

In the K_2O-SiO_2 diagram, these samples define a trend between 52% and 64% SiO_2 at high K_2O, and lie in the high-K calc-alkaline field. Other elements, such as MgO, Na_2O, FeO, TiO_2, Al_2O_3, and CaO, show the inverse correlation with SiO_2. These coherent chemical variations can be interpreted in terms of fractional crystallization processes (Wilson, 1989). In the SiO_2-MgO, CaO-MgO, and K_2O-MgO diagrams (Fig. 21), all the samples fall in between factional crystallization of olivine and fractional

Table 2

Major and trace element concentrations from Heikongshan whole-rock analysis of sample Hei-10009. FeO* represents the total iron.

	wt.%		ppm		ppm		ppm
SiO_2	54.36	La	46.13	Er	3.09	U	1.73
TiO_2	1.43	Ce	88.38	Tm	0.44	Pb	13.15
Al_2O_3	17.26	Pr	9.97	Yb	2.69	Rb	57.20
FeO*	8.17	Nd	36.10	Lu	0.42	Cs	0.70
MnO	0.14	Sm	6.92	Ba	521.00	Sr	451.00
MgO	4.50	Eu	1.81	Th	17.78	Sc	20.70
CaO	6.84	Gd	6.20	Nb	23.41	Zr	225.00
Na_2O	4.03	Tb	0.99	Y	29.94		
K_2O	2.70	Dy	5.88	Hf	5.28		
P_2O_5	0.39	Ho	1.17	Ta	1.40		

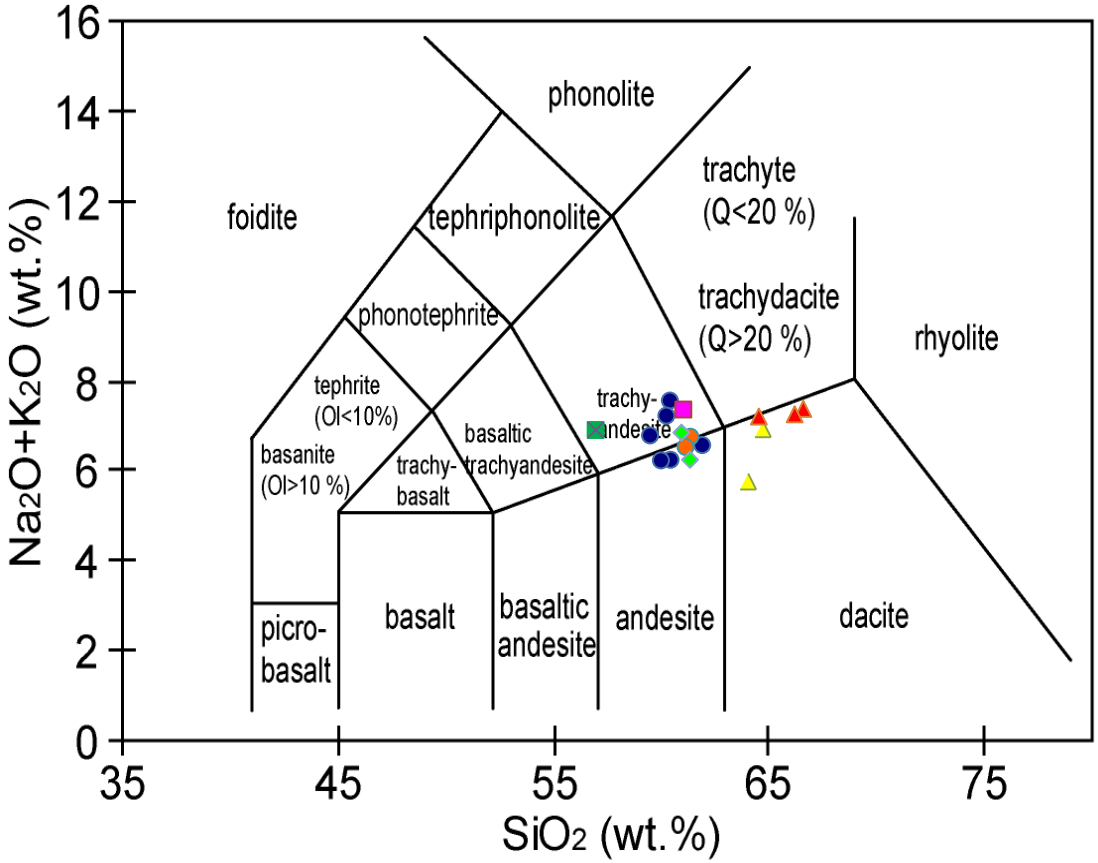

Figure 18. Total Alkalis-Silica (TAS) diagram (Le Maitre et al., 1989) of the Tengchong Holocene volcanic rocks. Green square denotes sample from Heikongshan (this study), light green diamonds denote samples from Heikongshan (Zhao et al., 2010), pink square denotes sample from Maanshan (Zou et al., 2010), orange circles denote samples from Maanshan (Zhao et al., 2010), blue circles denote sample from Maanshan (Wang et al., 2006), red triangles denote samples from Dayingshan (Zhao et al., 2010), and yellow triangles denote samples from Dayingshan (Wang et al., 2006).

Table 3

Major element compositions for Heikongshan, Dayingshan, and Maanshan volcanic rocks. The samples (MF1-MF5, MA02, 08YTC01-08YTC04) from Maanshan (Wang et al., 2006; Zou et al., 2010; Zhao et al., 2010), samples (DF2-DF3, 08YTC14-08YTC17) from Dayingshan (Wang et al., 2006; Zhao et al., 2010) and samples (Hei-10009, 08YTC11-08YTC13) from Heikongshan (in this paper; Zhao et al., 2010) are presented here for the purpose of reference.

	Maanshan								
	MF1	**MF2**	**MF3-1**	**MF3-2**	**MF4**	**MF5**	**MA02**	**08YTC01**	**08YTC04**
SiO_2	57.87	57.42	56.91	57.83	57.67	59.34	58.46	58.79	58.56
TiO_2	1.17	1.23	1.03	1.11	1.17	1.19	1.17	1.36	1.40
Al_2O_3	16.63	17.18	17.44	16.02	17.17	17.06	16.56	16.76	16.93
FeO	6.69	6.35	6.73	6.46	5.83	5.48	5.85	4.81	4.67
MnO	0.13	0.12	0.15	0.17	0.15	0.10	0.11	0.11	0.11
MgO	4.35	3.76	3.88	4.02	3.55	3.12	3.49	3.76	3.74
CaO	6.74	6.09	6.43	5.52	6.00	5.64	5.58	5.63	5.94
Na_2O	3.50	3.31	3.17	3.79	3.50	3.22	3.79	3.58	3.46
K_2O	2.56	2.74	3.44	3.60	3.55	3.17	3.40	3.00	2.89
P_2O_5	0.42	0.41	0.43	0.45	0.39	0.34	0.46	0.47	0.47

Table 3 continued

Major element compositions for Heikongshan, Dayingshan, and Maanshan volcanic rocks. The samples (MF1-MF5, MA02, 08YTC01-08YTC04) from Maanshan (Wang et al., 2006; Zou et al., 2010; Zhao et al., 2010), samples (DF2-DF3, 08YTC14-08YTC17) from Dayingshan (Wang et al., 2006; Zhao et al., 2010) and samples (Hei-10009, 08YTC11-08YTC13) from Heikongshan (in this paper; Zhao et al., 2010) are presented here for the purpose of reference.

	Dayingshan					Heikongshan		
	DF2	**DF3**	**08YTC14**	**08YTC15**	**08YTC17**	**Hei-10009**	**08YTC11**	**08YTC13**
SiO_2	61.48	62.17	64.06	61.98	63.65	54.36	58.77	58.37
TiO_2	0.92	0.98	1.00	1.18	1.04	1.43	1.33	1.41
Al_2O_3	16.22	16.48	15.86	16.36	16.07	17.26	16.75	17.13
FeO	5.65	5.21	3.48	4.07	3.51	8.17	4.96	3.79
MnO	0.11	0.16	0.09	0.09	0.09	0.14	0.11	0.10
MgO	3.08	2.59	2.17	2.66	2.27	4.50	4.24	3.58
CaO	4.97	5.35	3.90	4.77	4.11	6.84	5.98	5.95
Na_2O	2.09	2.90	3.51	3.48	3.35	4.03	3.30	3.52
K_2O	3.49	3.85	3.69	3.55	3.73	2.70	2.76	3.15
P_2O_5	0.42	0.42	0.33	0.40	0.35	0.39	0.45	0.48

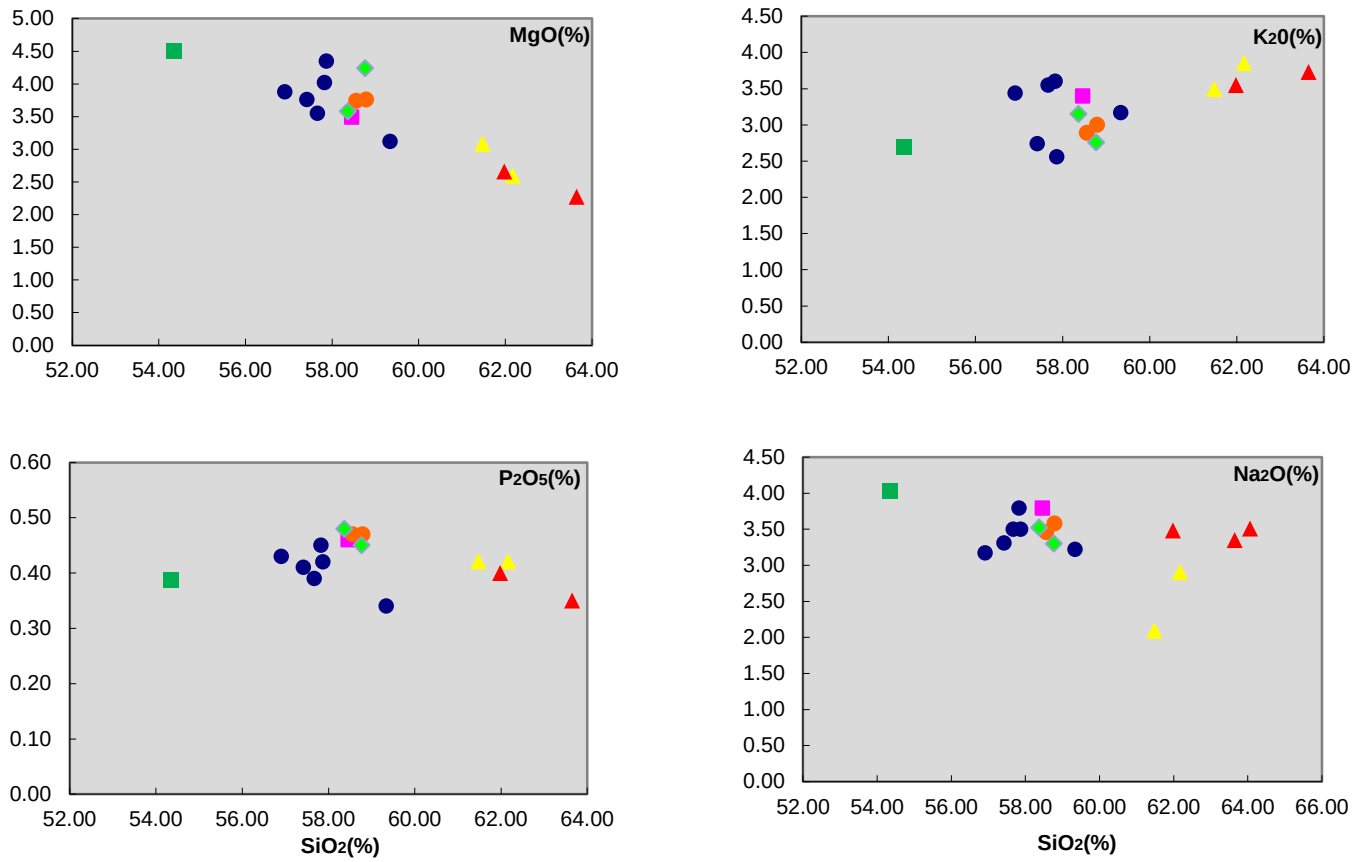

Figure 19. Harker Diagram of MgO, K_2O, P_2O_5, and Na_2O vs. SiO_2. Green square denotes sample from Heikongshan (this study), light green diamonds denote samples from Heikongshan (Zhao et al., 2010), pink square denotes sample from Maanshan (Zou et al., 2010), orange circles denote samples from Maanshan (Zhao et al., 2010), blue circles denote sample from Maanshan (Wang et al., 2006), red triangles denote samples from Dayingshan (Zhao et al., 2010), and yellow triangles denote samples from Dayingshan (Wang et al., 2006).

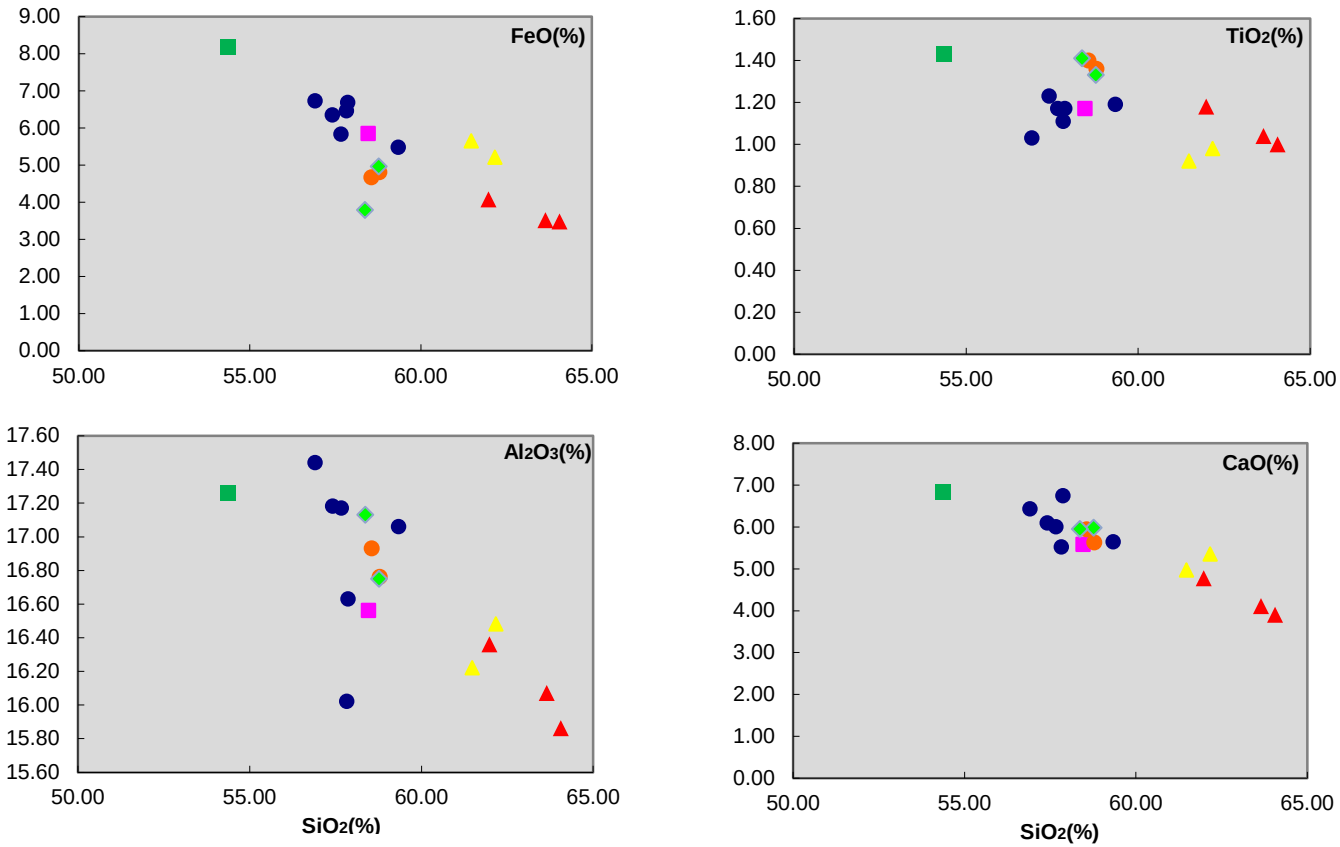

Figure 20. Harker Diagram of FeO, TiO_2, Al_2O_3, and CaO vs. SiO_2. Green square denotes sample from Heikongshan (this study), light green diamonds denote samples from Heikongshan (Zhao et al., 2010), pink square denotes sample from Maanshan (Zou et al., 2010), orange circles denote samples from Maanshan (Zhao et al., 2010), blue circles denote sample from Maanshan (Wang et al., 2006), red triangles denote samples from Dayingshan (Zhao et al., 2010), and yellow triangles denote samples from Dayingshan (Wang et al., 2006).

crystallization of olivine and clinopyroxene, which can be interpreted that the magma might have evolved before entering into the magma reservoir, and large amounts of olivine had crystallized and clinopyroxenes started to crystallize. The Al_2O_3-SiO_2 and MgO-SiO_2 diagrams (Fig. 22) show the magma was in the phase crystallizing plagioclase. The TiO_2-SiO_2 and P_2O_5-SiO_2 diagram (Fig. 22) do not indicate the magma was in the phase cystallizing magnetites and apatites, respectively.

Based on the relationship between Al_2O_3 and CaO, K_2O and Na_2O, alumina saturation of volcanic rocks can be divided into peraluminous (Al_2O_3 > (CaO + K_2O + Na_2O)), metaluminous((CaO + K_2O + Na_2O) > Al_2O_3 > (K_2O + Na_2O)), and peralkaline (Al_2O_3 < (K_2O + Na_2O)). The Heikongshan rock sample is metaluminous. The alumina saturation index (ASI) molecular ratio (Al_2O_3/ (CaO + K_2O + Na_2O)) is 0.78 and Al_2O_3/ (K_2O + Na_2O) is 1.81. The solubility of Zr in peraluminous and metaluminous magma is relatively low comparing with Zr solubility in peralkaline magma (Zou and Fan, 2011), making it easier to grow zircons in the Heikongshan magmas.

The trace element data (Table 4) are one of the useful tools to distinguish petrogenetic processes. The rare earth elements (REE) are particularly useful in the petrogenetic studies of igneous rocks because they are geochemically similar. In order to eliminate the Oddo-Harkins effects and compare REE abundances, the concentrations of individual REE in a rock should be normalized to their abundances in average chondritic meteorites (Nakamura, 1974). Figure 23 illustrates a range of chondrite-normalized REE patterns for Heikongshan volcanic rock and the other Tengchong Holocene volcanic rocks. The REE plot shows a negative slope with high concentrations of light rare earth

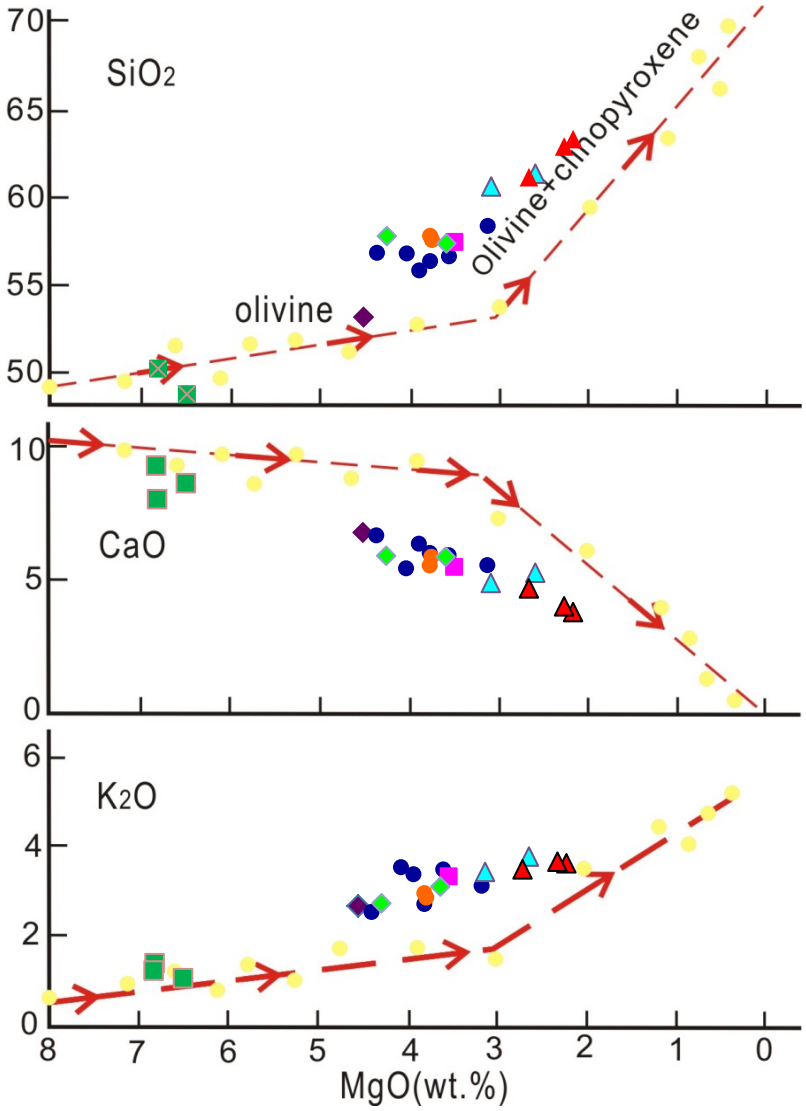

Figure 21. Plot showing the SiO_2, CaO, and K_2O vs. MgO relationships among the Tengchong Holocene volcanic rocks. Purple diamond denotes sample from Heikongshan (this study), light green diamonds denote samples from Heikongshan (Zhao et al., 2010), pink square denotes sample from Maanshan (Zou et al., 2010), orange circles denote samples from Maanshan (Zhao et al., 2010), dark blue circles denote sample from Maanshan (Wang et al., 2006), red triangles denote samples from Dayingshan (Zhao et al., 2010), light blue triangles denote samples from Dayingshan (Wang et al., 2006), and dark green squares denote Pliocene basalts in Tengchong volcanic field (Zhu et al., 1983).

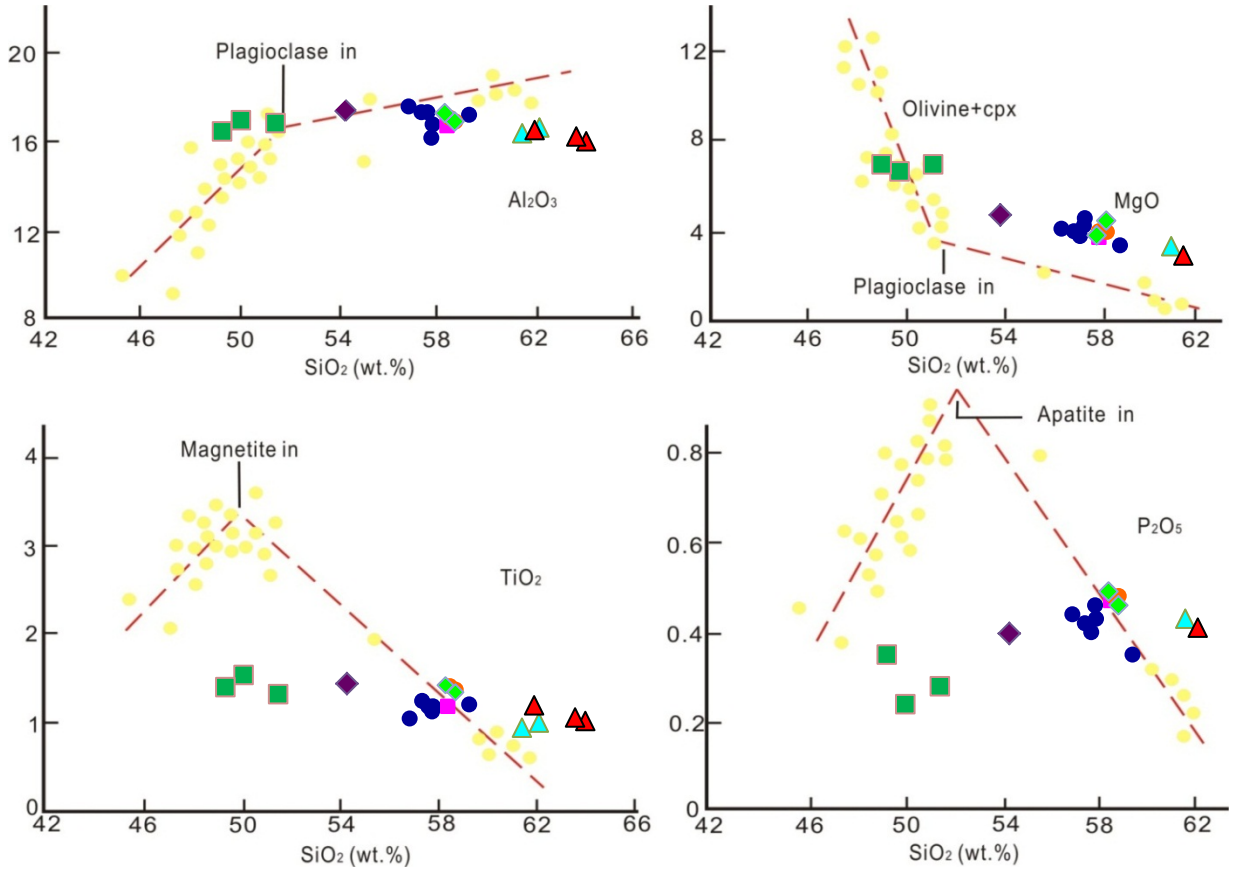

Figure 22. Harker variation diagrams for a suite of co-genetic volcanic rocks (dark blue circles) related by fractional crystallization of olive, clinopyroxene, plagioclase, magnetite and apatite (Wilson, 1989). Purple diamond denotes sample from Heikongshan (this study), light green diamonds denote samples from Heikongshan (Zhao et al., 2010), pink square denotes sample from Maanshan (Zou et al., 2010), orange circles denote samples from Maanshan (Zhao et al., 2010), dark blue circles denote sample from Maanshan (Wang et al., 2006), red triangles denote samples from Dayingshan (Zhao et al., 2010), light blue triangles denote samples from Dayingshan (Wang et al., 2006), and dark green squares denote Pliocene basalts in Tengchong volcanic field (Zhu et al., 1983).

Table 4

Trace element concentration (ppm) for Heikongshan, Dayingshan, and Maanshan volcanic rocks. The samples (MA02, 08YTC01) from Maanshan (Zou et al., 2010; Zhao et al., 2010), samples (YTC9724-5, 08YTC15) from Dayingshan (Tucker, 2011; Zhao et al., 2010) and samples (Hei-10009, 08YTC11) from Heikongshan (in this paper; Zhao et al., 2010) are presented here for the purpose of reference. Symbol "–" represent not analyzed.

	Maanshan		Dayingshan		Heikongshan	
	MA02	**08YTC01**	**YTC9724-5**	**08YTC15**	**Hei-10009**	**08YTC11**
Cs	1.44	1.94	2.02	2.06	0.7	1.32
Rb	105	105	150.3	127	57.2	99
Ba	764	780	865	897	521	928
Th	17.5	33.9	34.32	32.7	17.78	23.3
U	2.56	—	3.32	—	1.73	—
Nb	27.1	27	27.6	27.3	23.41	28
Ta	1.65	1.67	2.69	1.72	1.4	1.66
La	65	65.9	79.22	78.4	46.13	73.7
Ce	123	125	151.4	154	88.38	145
Pb	19.1	20.1	25.57	26.1	13.15	22.6
Pr	13.5	14.3	16.37	17.2	9.97	16.6
Sr	574	534	445	433	451	523
Nd	48.5	49.5	57.19	59.5	36.1	56.8
Zr	260	313	303	320	225	311
Hf	6.53	8.64	8.13	9.4	5.28	8.89
Sm	8.79	8.73	9.79	10	6.92	9.73
Eu	1.92	1.79	1.82	1.78	1.81	1.93
Gd	7.07	7.05	7.4	7.4	6.2	7.06
Tb	1.05	0.98	1.08	1.05	0.99	1.02
Dy	5.94	5.62	5.97	5.82	5.88	5.53
Ho	1.14	1.11	1.14	1.12	1.17	1.07
Er	2.96	2.88	3	3.01	3.09	2.8
Yb	2.61	2.73	2.6	2.6	2.69	2.42
Y	29.2	27.1	29.27	27.2	29.94	26.1
Lu	0.4	0.42	0.4	0.41	0.42	0.38

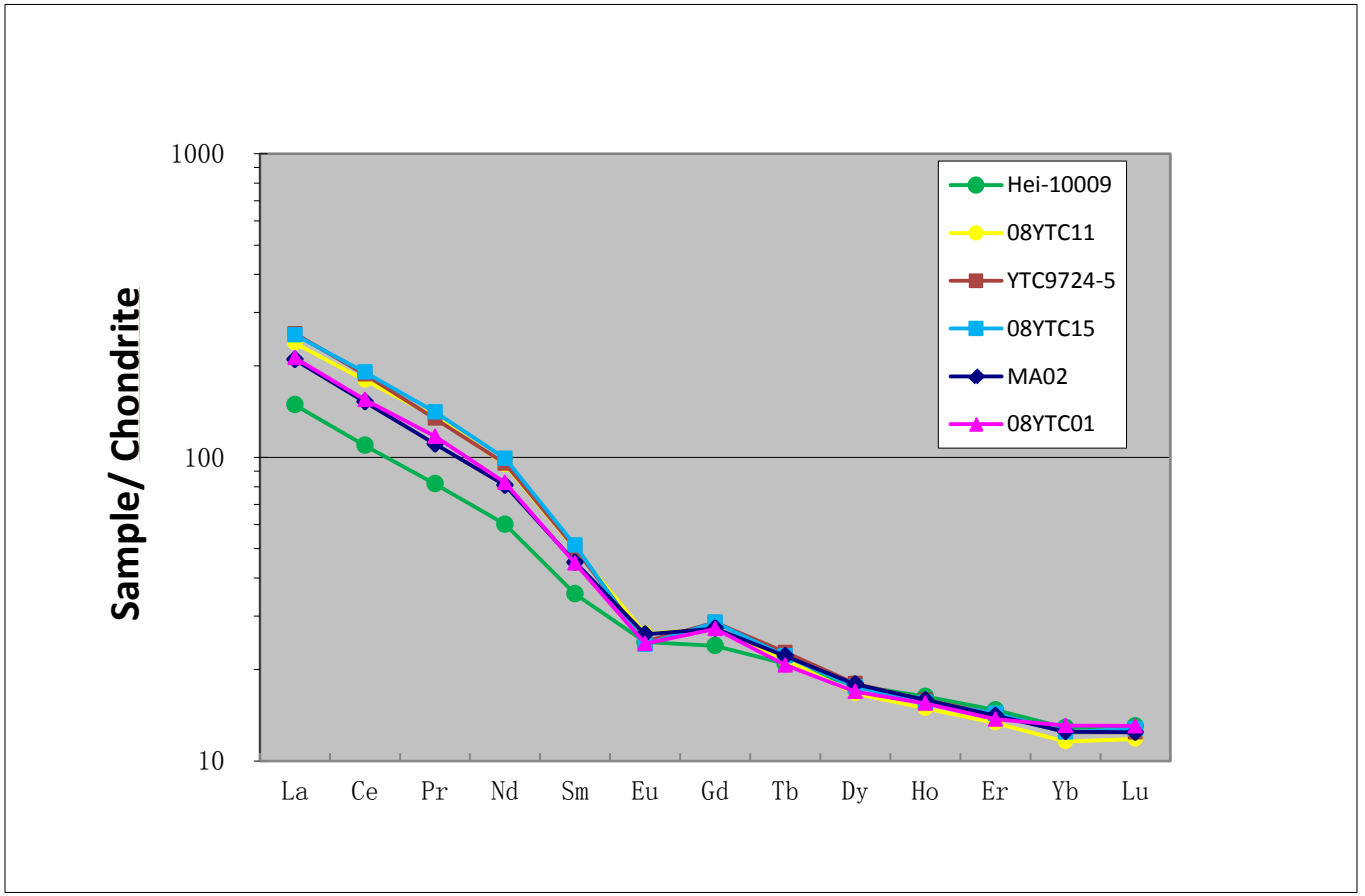

Figure 23. Chondrite-normalized REE patterns of the Heikongshan, Dayingshan, and Maanshan volcanic rocks. Data are from Zhao et al. (2010), Zou et al. (2010), Tucker (2011) and this study. Chondrite-normalized values are after Nakamura, 1974.

elements (light-REE) and low concentrations of heavy rare earth elements (heavy-REE). This may suggest the presence of residual garnet in the source. The extremely high concentrations of light-REE may suggest very small degrees of partial melting (Wilson, 1989). These volcanic rocks show a slight negative Eu anomaly, which means they may have fractionally crystallized plagioclases.

In order to better understand the pattern of trace element abundances in these samples, the elements Ba, Sr, U, Th, Zr, Nb, Ti and REE are plotted to develop the spider diagram (Fig. 24). The concentrations of these elements are normalized to their abundances in average primitive mantle. From the spider diagram, the samples exhibit negative Sr, Nb, and Ta anomalies. The negative Sr anomalies may result from the fractional crystallization of plagioclase (Wilson, 1989). The negative Nb and Ta anomalies may result from partial melting of a mantle source metasomatized by hydrous fluids from the subducting plate. Unlike many other elements (e.g., U, Ba), Nb and Ta are not soluble in subduction-related hydrous fluids. Subduction-related fluids dominate the trace element budgets in magmas, therefore, the subduction-related magmas would be depleted in Nb and Ta.

Whole-Rock Nd-Sr-Pb Isotopes

The Sr-Nd-Pb isotopic data (Table 5 and Table 6) were compiled from Zhu et al. (1983), Wang et al. (2006), Zou et al. (2010) and Zhao et al. (2010). These samples have $^{87}Sr/^{86}Sr$ ratios of 0.705950~0.711243 and $^{143}Nd/^{144}Nd$ ratios of 0.502360~0.512604. In the $^{143}Nd/^{144}Nd$-$^{87}Sr/^{86}Sr$ diagram (Fig. 25), these isotopic compositions from the Tengchong volcanic rocks indicate an enriched mantle source. The ranges of Pb isotopic ratios of the

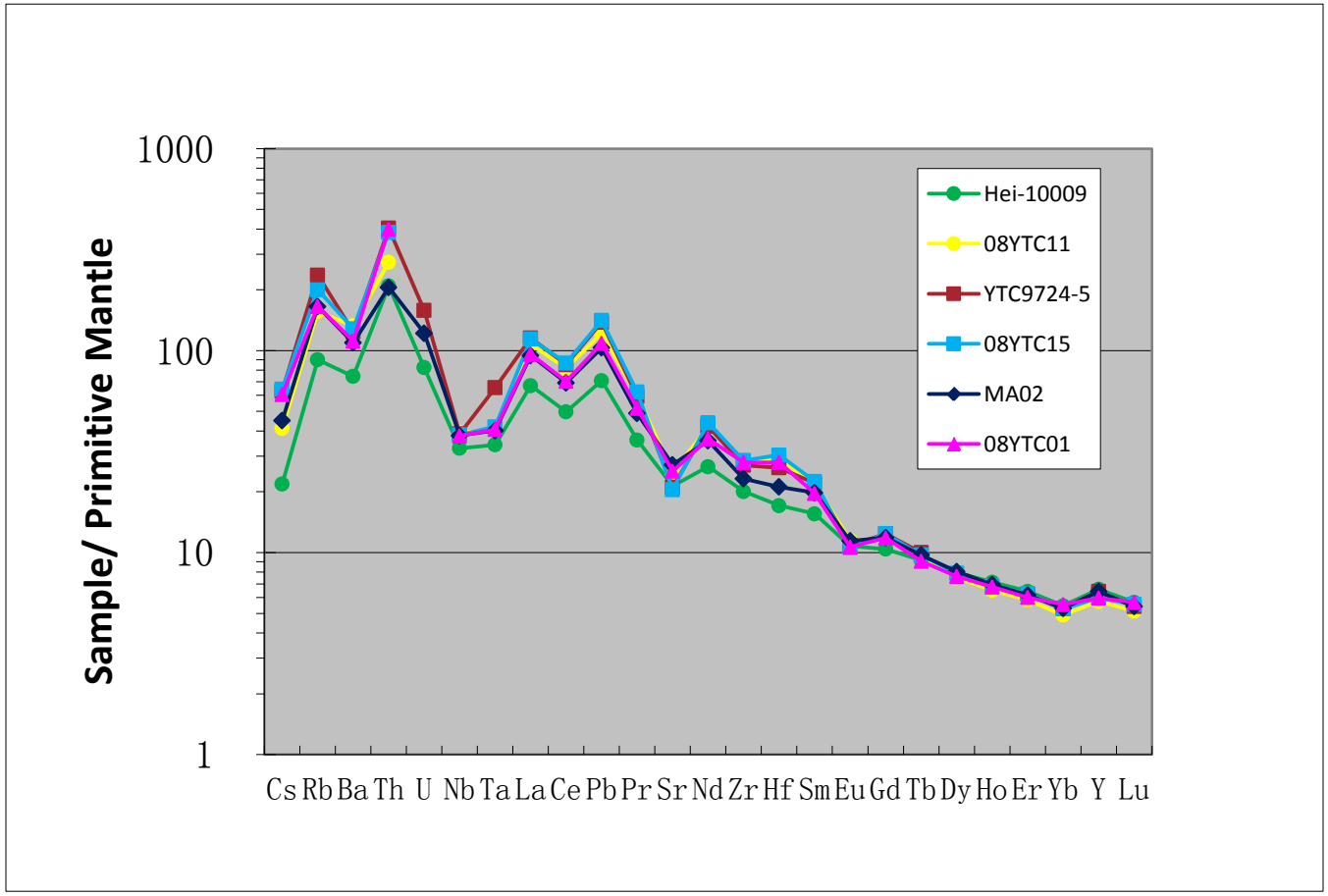

Figure 24. Trace element spider diagram of the Heikongshan, Dayingshan, and Maanshan volcanic rocks. Data are from from Zhao et al. (2010), Zou et al. (2010), Tucker (2011) and this study. Primitive mantle-normalized values are from Sun and McDonough (1989).

Table 5

Sr-Nd isotopic compositons for the Tengchong volcanic rocks. The samples (08YTC01~08YTC15) from Zhao et al. (2010), sample (MA02) from Zou et al. (2010), samples (MF1~DF3) from Wang et al. (2006), and samples (TV-4~TV-102) from Zhu et al. (1983) are presented here for the purpose of reference.

	$^{87}Sr/^{86}Sr$	$^{143}Nd/^{144}Nd$		$^{87}Sr/^{86}Sr$	$^{143}Nd/^{144}Nd$
08YTC01	0.707528	0.512296	TV-4	0.708807	0.512225
08YTC11	0.708553	0.512213	TV-10	0.708514	0.512227
08YTC15	0.708919	0.512170	TV-15	0.706721	0.512346
MA02	0.707556	0.512281	TV-23	0.705957	0.502360
MF1	0.707450	0.512224	TV-25	0.706454	0.512441
MF2	0.707240	0.512227	TV-28	0.711243	0.511936
MF3-1	0.706490	0.512421	TV-32	0.709253	0.512032
MF3-2	0.706670	0.512366	TV-33	0.708130	0.512230
MF4	0.707540	0.512454	TV-35	0.707146	0.512463
MF5	0.706890	0.512032	TV-38	0.708030	0.512456
DF2	0.708540	0.512066	TV-40	0.706911	0.512497
DF3	0.707400	0.512346	TV-102	0.705950	0.512604

Table 6

Pb isotopic compositons for the Tengchong volcanic rocks. The samples (08YTC01~08YTC15) from Zhao et al. (2010), sample (MA02) from Zou et al. (2010), and samples (MF1~DF3) from Wang et al. (2006) are presented here for the purpose of reference.

	Heikongshan	Dayingshan	Maanshan	
	08YTC11	08YTC15	08YTC01	MA02
$^{206}Pb/^{204}Pb$	18.0443	18.0533	18.1269	18.1630
$^{207}Pb/^{204}Pb$	15.6473	15.6451	15.6426	15.6810
$^{208}Pb/^{204}Pb$	39.0509	39.0643	39.0601	39.1920

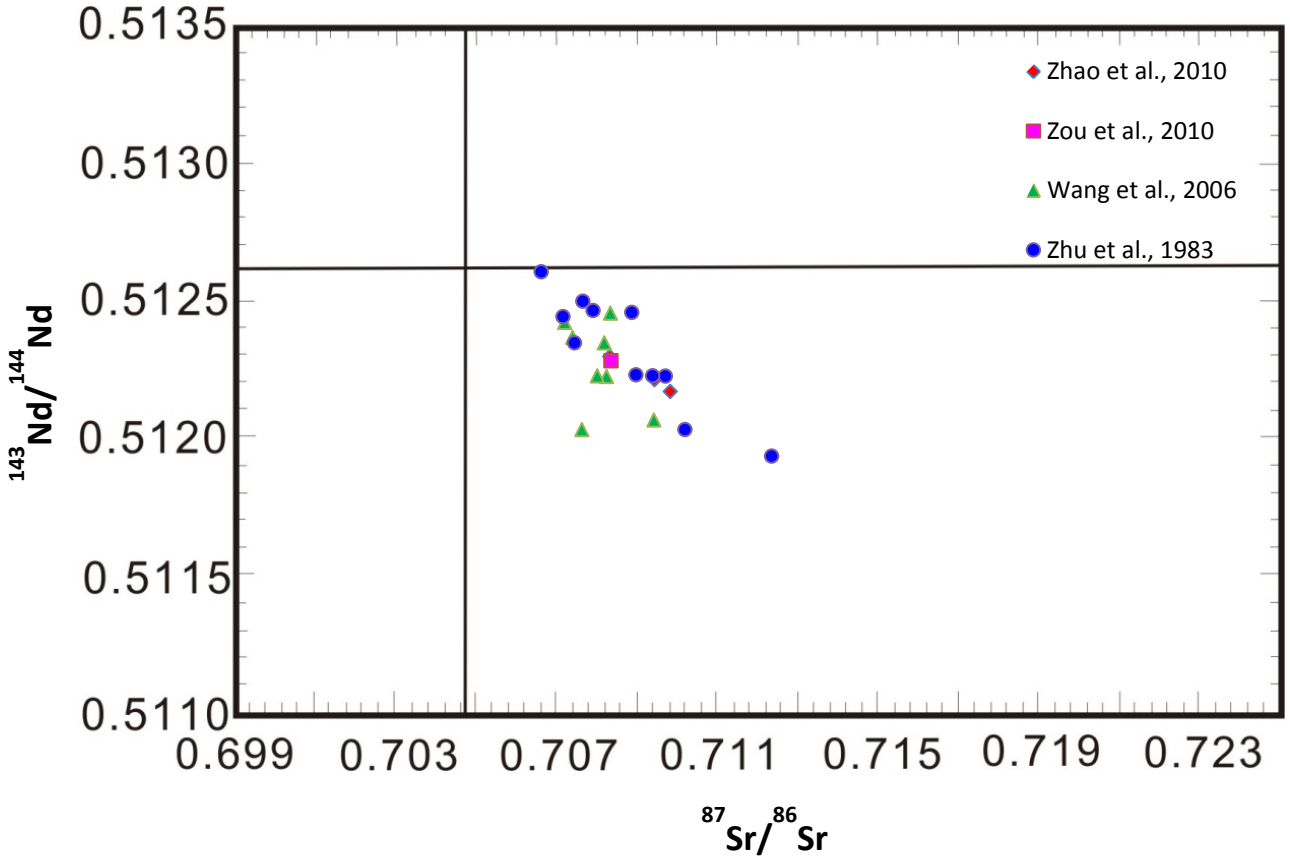

Figure 25. $^{143}Nd/^{144}Nd$-$^{87}Sr/^{86}Sr$ diagram for the Tengchong volcanic rocks. Data are from Zhao et al. (2010), Zou et al. (2010), Wang et al. (2006) and Zhu et al. (1983).

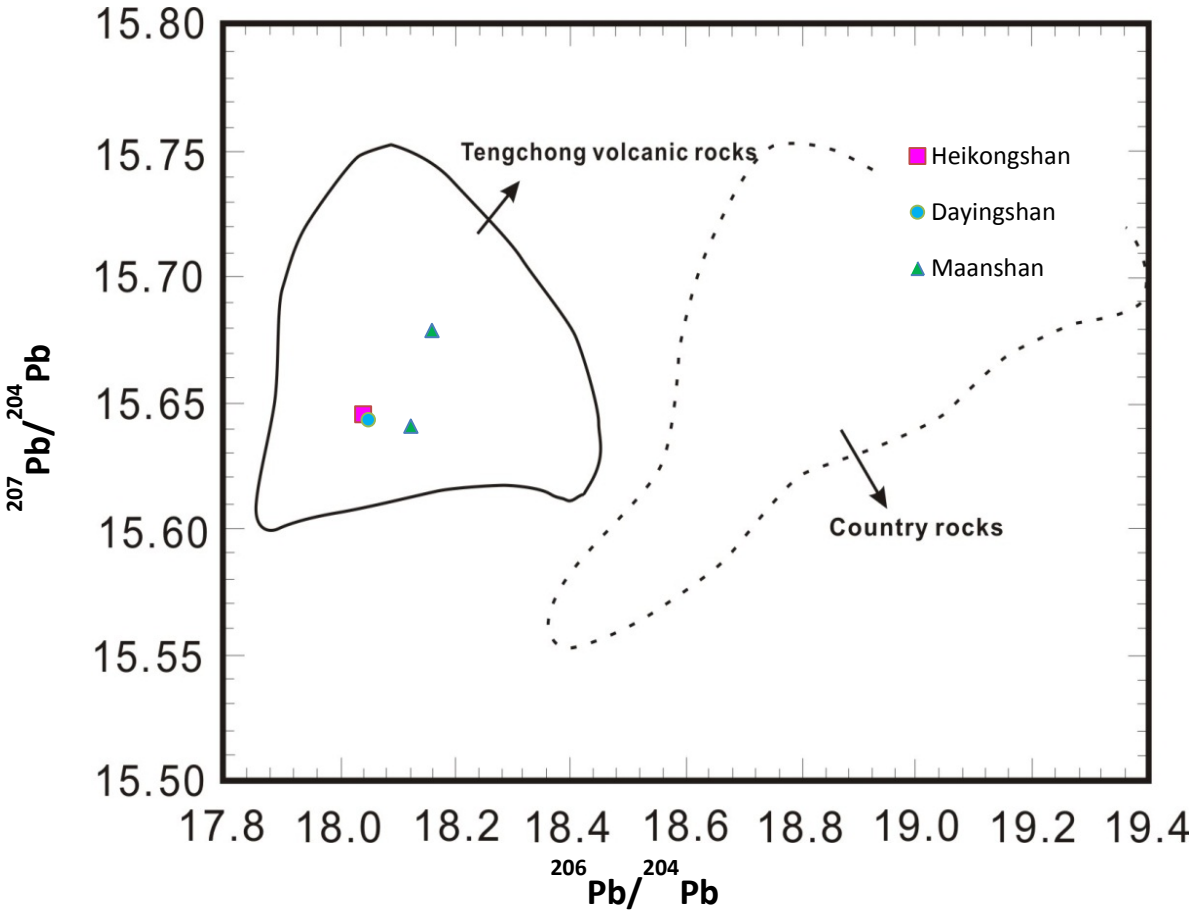

Figure 26. $^{207}Pb/^{204}Pb$-$^{206}Pb/^{204}Pb$ diagram for the Tengchong volcanic rocks. Data are from Zhao et al. (2010) and Zou et al. (2010)

samples are 18.044~18.163 for $^{206}Pb/^{204}Pb$, 15.643~15.681 for $^{207}Pb/^{204}Pb$, and 39.051~39.192 for $^{208}Pb/^{204}Pb$. In the $^{207}Pb/^{204}Pb$-$^{206}Pb/^{204}Pb$ diagram (Fig. 26), the Tengchong volcanic rocks are clearly different from their country rocks, indicating that they were not significantly contaminated by the country rocks (Chen et al., 2002).

Heikongshan Zircon U-Th Ages

Most Heikongshan zircons do not have well-developed growth-zoning, and only two of them show growth-zoning. 19 zircon grains were selected and 24 spots were measured (Table 7) for SIMS analysis. Using mixture modeling of U-Th zircon-whole-rock two-point model ages (Sambridge and Compston, 1994) and the probability density function from Isoplot (Ludwig, 2003), the Heikongshan zircons yield a bi-modal population with model ages of 67.3 ± 14 ka and 99.9 ± 4.6 ka (Fig. 27) in the proportions of 19% and 81%, respectively. The mixture modeling method is an effective approach detecting multiple components in a population of analytical observations for zircon and other ages. Using this method it can estimate the most likely ages, proportions and number of distinct components in a given dataset (Sambridge and Compston, 1994). The older 99.9 ka population is dominant, and the 67 ka peak is a minor one with large uncertainty in model age.

If all zircons are taken together, we obtain an isochron age of 102.7 ± 7.9 ka with MSWD of 1.9 (Fig. 28). Note that isochon ages are more dependent on the high U/Th zircons. Several zircon grains with young model ages and low U/Th ratios play only minor roles in determining isochron ages.

Table 7

U/Th isotope data, concentrations and ages for Heikongshan zircons measured by SIMS. 1s is the standard error and is a measurement of uncertainty. Isoplot (Ludwig, 2003) is used for calculation of ages.

Sample	($^{238}U/^{232}Th$)	1s	($^{230}Th/^{232}Th$)	1s	U(ppm)	Th(ppm)	Th/U	$D_{Th/U}$	Age(ka)	+ (ka)	- (ka)
2011_08_20Aug\ Hei@1.ais	1.770	0.033	1.230	0.031	843	1366	1.62	0.158	99.2	7.1	-6.7
2011_08_20Aug\ Hei@2.ais	1.280	0.023	0.948	0.030	344	548	1.59	0.155	102.2	10.2	-9.4
2011_08_20Aug\ Hei@3.ais	1.547	0.028	1.178	0.031	1290	1881	1.46	0.142	119.1	10.3	-9.4
2011_08_20Aug\ Hei@4.ais	1.328	0.024	0.939	0.020	723	1228	1.70	0.165	92.0	6.5	-6.1
2011_08_20Aug\ Hei@5.ais	0.974	0.020	0.655	0.040	175	386	2.20	0.215	63.1	13.2	-11.8
2011_08_20Aug\ Hei@7.ais	1.985	0.036	1.370	0.042	466	747	1.60	0.156	101.2	8.3	-7.7
2011_08_20Aug\ Hei@8.ais	1.284	0.024	0.916	0.024	803	1360	1.69	0.165	92.5	7.8	-7.3
2011_08_20Aug\ Hei@9.ais	1.082	0.020	0.742	0.033	203	399	1.96	0.191	74.1	10.6	-9.7
2011_08_20Aug\ Hei@11.ais	2.232	0.040	1.509	0.093	164	265	1.62	0.157	99.8	14.9	-13.1
2011_08_20Aug\ Hei@12.ais	1.469	0.027	1.114	0.037	365	540	1.48	0.144	115.8	12.1	-10.9
2011_08_20Aug\ Hei@13.ais	1.118	0.022	0.745	0.037	176	360	2.04	0.199	70.0	10.8	-9.9
2011_08_20Aug\ Hei@15.ais	2.703	0.106	1.738	0.070	1242	2085	1.68	0.163	93.8	10.6	-9.7
2011_08_20Aug\ Hei@16.ais	1.921	0.039	1.390	0.047	605	913	1.51	0.147	111.9	10.8	-9.9
2011_08_20Aug\ Hei@17.ais	1.963	0.035	1.272	0.069	241	424	1.75	0.171	87.6	11.3	-10.3
2011_08_20Aug\ Hei@18.ais	1.564	0.033	1.031	0.134	46	84	1.81	0.176	83.6	29.6	-23.3
2011_08_20Aug\ Hei@5sp2.ais	0.910	0.028	0.656	0.045	247	488	1.97	0.192	73.7	19.4	-16.5
2011_08_20Aug\ Hei@3sp2.ais	1.639	0.030	1.211	0.023	846	1275	1.51	0.147	112.4	7.3	-6.8
2011_08_20Aug\ Hei@12sp2.ais	1.284	0.024	0.932	0.036	319	524	1.64	0.160	97.2	11.5	-10.4
2011_08_20Aug\ Hei@11sp2.ais	3.096	0.094	2.147	0.072	444	668	1.51	0.147	112.3	11.0	-10.0
2011_08_20Aug\ Hei@8sp2.ais	1.355	0.024	0.978	0.020	941	1537	1.63	0.159	98.0	6.8	-6.4
2011_08_20Aug\ Hei@9sp2.ais	1.281	0.027	0.908	0.044	247	423	1.71	0.167	90.8	13.3	-11.8
2011_08_20Aug\ Hei@19.ais	0.533	0.010	0.441	0.017	462	1330	2.88	0.280	44.7	16.0	-14.0
2011_08_20Aug\ Hei@4sp2.ais	1.793	0.032	1.235	0.037	592	970	1.64	0.159	97.7	8.0	-7.4

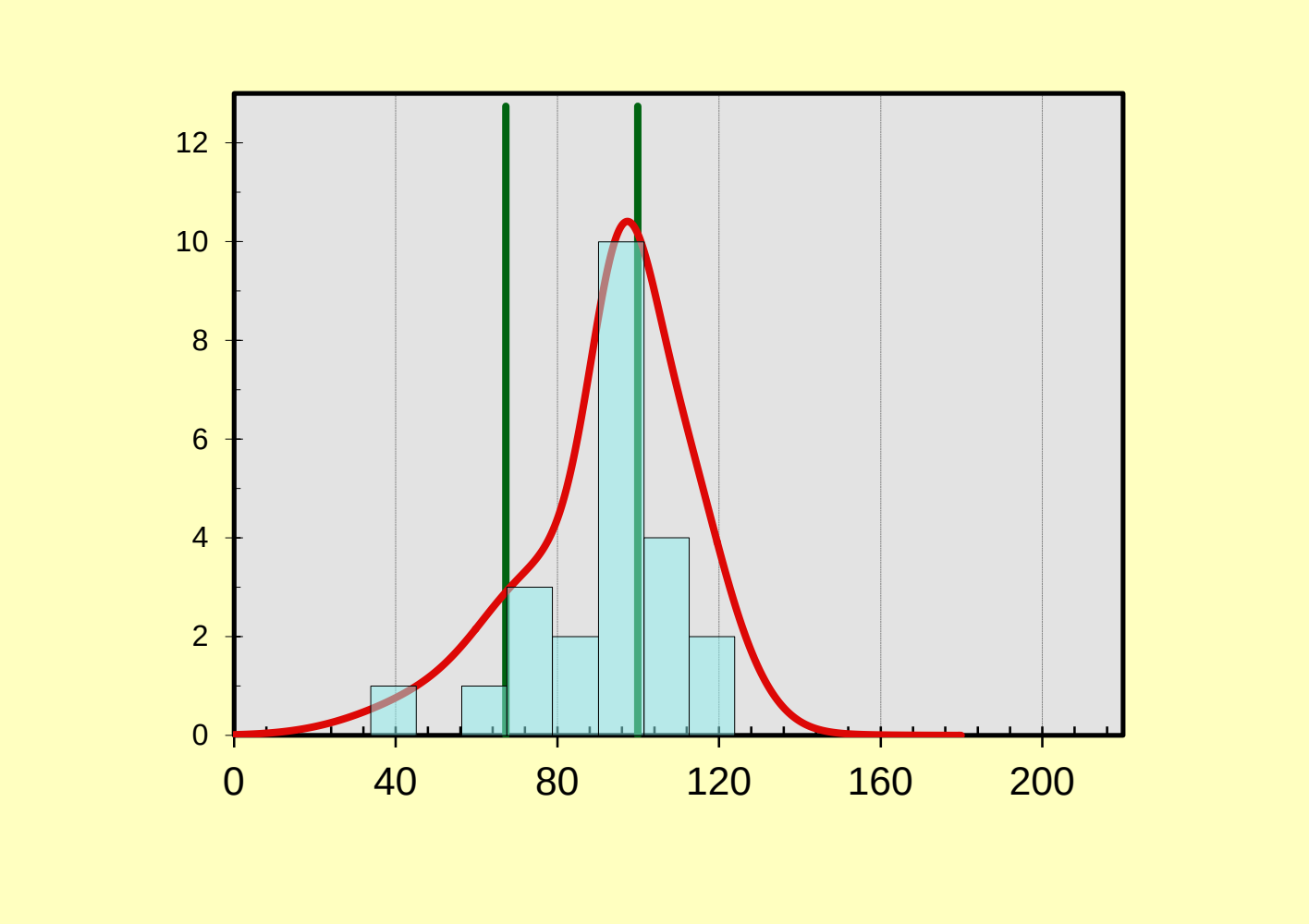

Figure 27. Mixture modeling of U-Th ages of zircon crystals from Heikongshan from Isoplot (Ludwig, 2003). The horizontal axis is in ka. The two green vertical lines represent two age populations at 67.3 and 99.9 ka, respectively.

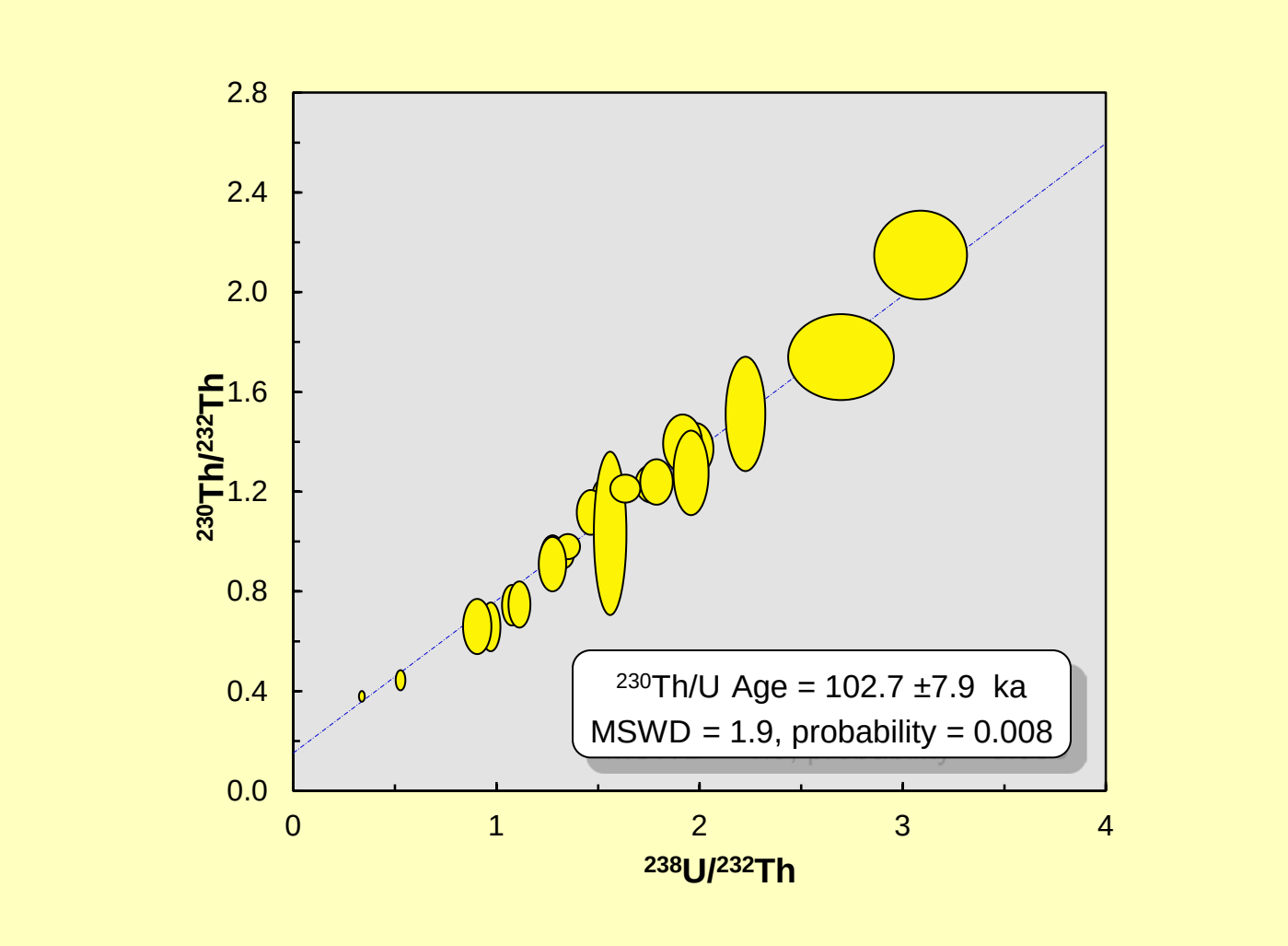

Figure 28. U/Th isochron plot for zircons from Heikongshan. Chart was constructed and ages were determined using Isoplot (Ludwig, 2003). Data-point error ellipses are 2σ.

Zircon Saturation Temperature

The reason why geochronologists prefer to use zircon crystals as an effective dating tool is due to its stability over long periods of geologic time (Heaman and Parrish, 1991; Dickin, 1995). Zircon saturation temperature in magmas can be estimated from the whole-rock composition and Zr concentrations in magmas. Hydrothermal experiments have defined the zircon saturation in magmas as a function of temperature and magma composition by the following equation (Watson and Harrison, 1983):

$$\ln D_{\mathrm{Zr}}^{\mathrm{Zircon/melt}} = \{-3.80-[0.85(M-1)]\} + \frac{12900}{T},$$

where $D_{Zr}^{zircon/melt}$ represents the concentration ratio in zircon to that in the melt (in ppm), T is the absolute temperature (in Kelvin), and M is the cation ratio (Na + K +2Ca)/ (Al * Si). For the Heikongshan sample in this study, M is 2.54. The whole-rock (melt) analysis yielded a Zr concentration of 225 ppm. Using the above model to estimate the magma temperature, the average zircon saturation temperature is about 735 °C, which is close to the previous estimate temperature of 750 °C based on Ti-in-zircon geothermometry from Maanshan (Zou et al., 2010).

DISCUSSION

Magma Chamber Storage Time

The study of the pre-eruptive history of magma is fundamental to understanding the magmatic evolution that leads to volcanic eruptions. Ion microprobe dating of zircons indeed unravels the time scales of crystallization and storage of the magma beneath Tibetan Plateau. Using primarily ion microprobe ^{238}U-^{230}Th ages of zircons from the Heikongshan volcanic rocks, unique constraints are placed on the crystallization history of the potassic lavas at Heikongshan. Pre-eruption magma residence time scales can be inferred from the difference between magma eruption age and zircon crystallization age (Reid et al., 1997). Mixture modeling of U-Th Hekongshan zircon ages yields a bi-modal age population of 67.3 ± 14 ka and 99.9 ± 4.6 ka, which represent two stages of zircon crystallization. Using an eruption age of < 10 ka, the magma chamber storage time is at least 57.3 ka.

Th/U Ratios in Zircons

The Heikongshan zircons have Th/U ratios ranging from 1.46 to 2.88, which are much higher than average Th/U ratios in most igneous zircons (about 0.5) (Bindeman et al., 2006). The high Th/U ratios in zircons may result from the high Th/U ratios in the

magma of the Heikongshan (Zou et al., 2010). From the trace elements analysis, the Heikongshan lavas have Th and U concentrations of 17.78 ppm and 1.73 ppm, respectively. The zircon/melt partitioning coefficients ($D_{Th/U}$) can be determined by the following equation:

$$D_{Th/U} = \frac{D_{Th}}{D_U} = \frac{Th_{zircon} / Th_{melt}}{U_{zircon} / U_{melt}} = \frac{Th_{zircon} / U_{zircon}}{Th_{melt} / U_{melt}}.$$

According to above equation, the $D_{Th/U}$ can be calculated using Th/U ratio in zircons divided by Th/U ratio in the melt. The Th/ U ratio in the melt is 10.28. The Th/U ratios in Heikongshan zircons (Table 4) were calculated from Th and U concentrations in zircons measured by SIMS. The $D_{Th/U}$ ranges from 0.142 to 0.215 for the Heikongshan zircons.

Magma Origin and Magma Evolution

Major and trace element analysis of the Heikongshan basaltic trachyandesite indicate that the magma was in the phase of crystallizing plagioclase and clinopyroxene. Yu et al. (2010) studied mafic and ultramafic autoliths in the Heikongshan volcanic rocks and suggested that their origin of these autoliths is related to magma evolution and eruption processes. They pointed out the primitive basaltic magma came from upper mantle, but did not directly erupt to the surface and was stored in the magma chamber in the crust. These autoliths have the same source as phenocrysts in the rock, and were derived from magmatic crystallization and fractional crystallization. Combining the lithology study of the Heikongshan lavas with the major element analysis in this study, the magma may have evolved and had crystallized large amounts of olivine before

entering into the magma chamber. This may indicate that the magmatic evolution of Heikongshan volcano is closely related to fractional crystallization.

Trace element concentration and isotopic composition analysis indicate the Tenngchong volcanic rocks originated from an enriched source (Zhu et al., 1983; Wang et al., 2006; Zou et al., 2010). Continental subduction may be the origin of the Tengchong volcanic rocks. In addition, paleomagnetic data reveals that a north-dipping previous subduction zone existed to the south of the crustal segment carrying the Tengchong volcanics before the India-Asia collision (Zhu at al., 1983). Thus the primitive basaltic magma from the source probably came from melting of upper mantle caused by previous north-dipping subduction.

CONCLUSIONS

(1) The Heikongshan zircons have two age populations at 67.3 ± 14 ka and 99.9 ± 4.6 ka. The dominant older ~99.9 ka peak represents remobilized zircon antecrysts derived from an earlier phase of basaltic magmatism, which remobilized into a later phase of magmatism. The younger ~67.3 ka peak represents zircon phenocrysts that grew in the most recent magma body before the eruption. Given an eruption age of ~10 ka, the magma storage time is at least 57 ± 14 ka for the basaltic trachyandesite from Heikongshan.

(2) Trace element concentration and isotopic composition analysis indicate that the Tenngchong volcanic rocks were derived from partial melting of an enriched mantle source metasomatized by previous north-dipping subduction.

REFERENCES

Bindeman, I.N., Schmitt, A.K., Valley, J.W., 2006. U–Pb zircon geochronology of silicic tuffs from the Timber Mountain/Oasis Valley caldera complex, Nevada: rapid generation of large volume magmas by shallow-level remelting. Contributions to Mineralogy and Petrology 152, 649–665.

Blundy, J., Wood, B., 2003. Mineral-melt partitioning of uranium, thorium and their daughters. Uranium-series Geochemistry: Review in Mineralogy and Geochemistry 52, 59-123.

Cherniak, D.J., Hanchar, J.M., Watson, E.B., 1997. Diffusion of tetravalent cations in zircon, Contributions to Mineralogy and Petrology 127, 383-390.

Chen, F., Satir, M., Ji, J., Zhong, D., 2002. Nd–Sr–Pb isotopes of Tengchong Cenozoic volcanic rocks from western Yunnan, China: evidence for an enriched-mantle source. Journal of Asian Earth Sciences 21, 39–45.

Condomines, M., 1997. Dating recent volcanic rocks through ^{230}Th-^{238}U disequilibrium in accessory minerals: example of the Puy de Dome (French Massifc Central). Geology 25, 375-378.

Deng, W.M., 1978. A preliminary study on the petrology and petrochemistry of the Quaternary volcanic rocks of northern Tibet autonomous region. Acta Geologica Sinica 52, 148-162.

Dickin AP (1995) Radiogenic Isotope Geology. Cambridge University Press, New York, 490 p.

Ding, L., Kapp, P., Zhong, D.L., Deng, W.M., 2003. Cenozoic volcanism in Tibet: evidence from oceanic to continental subduction. Journal of Petrology 44, 1833-1865.

Fan, P.F., 1978. Outline of the tectonic evolution of southwestern China. Tectonophysics 45, 261-267.

Finch R. J. and Hanchar J. M. (2003) Structure and chemistry of zircon and zircon-group minerals. Zircon Reviews in Mineralogy and Geochemistry 53, 1-25.

Flower, M.F., Tamaki, K., Hoang, N., 1998. Mantle extrusion: a model for dispersed volcanism and DUPAL-like asthenosphere in East Asia and the West Pacific. In: Flower, M.F.J., Chung, S.L., Lo, C.H., Lee, T.Y. (Eds.), Mantle Dynamics and Plate Interaction in East Asia. Am. Geophys. Union, Washington, D. C., pp. 67-88.

Fukuoka, T., 1974. Ionium dating of acidic volcanic rocks. Geochemical Journal 8, 109 -116.

Fukuoka, T., Kigoshi, K., 1974. Discordant Io-ages and the uranium and thorium distribution between zircon and host rocks. Geochemical Journal 8, 117-122.

Heaman L, Parrish RR (1991) U-Pb geochronology of accessory minerals. In Applications of radiogenic isotope systems to problems in geology. Short Course Handbook 19. Heaman L, Ludden JN (eds) Mineralogical Association of Canada, p 59-102.

Ireland, T.R., and Williams, I.S., 2003, Considerations in zircon geochronology by SIMS, in Hanchar, J.M., and Hoskin, P.W.O., eds., Zircon: Reviews in Mineralogy and Geochemistry 53, 215-241.

Le Maitre, R.W., 1979. A chemical approximation to the modal QAPF classification of the igneous rocks. Neues Jahrbuch fur Mineralogie, Abhandlungen, 136, 169-206.

Li, D.M., Li, Q., Chen, W.J., 2000. Volcanic activity of Tengchong since the Pliocene. Acta Petrologica Sinica 16, 362-370.

Liu R X, 2000. Active Volcanoes in China (in Chinese). Beijing: Seismological Press.
Monteleone, B.D., Baldwin, S.L., Webb, L.E., Fitzgerald, P.G., Grove, M., Schmitt, A.K., 2007. Late Miocene – Pliocene eclogite facies metamorphism, D'Entrecastreaux Islands, SE Papua New Guinea. Journal of Metamorphic Geology 25, 245-265.

Lowenstern, J.B., Persing, H.M., Wooden, J.L., Lanphere, M., Donnelly-Nolan, J., Grove, T. L., 2000. U-Th dating of single zircons from young granitoid xenoliths: new tools for understanding volcanic processes. Earth and Planetary Science Letters 183, 291-302.

Ludwig, K.R., 2003. User's Manual for ISOPLOT 3.00: a geochronological toolkit for Microsoft Excel. Berkeley Geochronology Center Special Publication No. 4, Berkeley.70 pp.

Miller, C., Schuster, R., Klotzli, U., Frank, W., Purtscheller, F., 1999. Post-collisional potassic and ultrapotassic magmatism in SW Tibet: geochemical and Sr-Nd-Pb-O isotopic constraints for mantle source characteristics and petrogenesis. Journal of Petrology 40, 1399-1424.

Nakamura N.1974: Determination of REE, Ba, Fe, Mg, Na and K in carbonaceous and ordinary chondrites. Geochimica et Cosmochimica Acta, 38, 757-775.

Paces, J.B., Miller, J.D., 1993. Precise U-Pb ages of Duluth complex and related mafic intrusions, northeastern Minnesota-geochronological insights to physical,petrogenetic,paleomagnetic, and tectonomagmatic processes associated with the 1.1 Ga midcontinent rift system. Journal of Geophysical Research 98, 13997–14013.

Powell, C.McA., Johnson, B.D., 1980. Constraints on the Cenozoic position of Sundaland. Tectonophysics 63, 91-109.

Pyle, D.M., Ivanovich, M., Sparkes, R.S.J., 1988. Magma-cumulate mixing identified by U-Th disequilibrium dating. Nature 331, 157-159.

Rowley, D.B., 1996, Age of initiation of collision between India and Asia: a review of stratigraphic data. Earth and Planetary Science Letter 145, 1-13.

Reid, M.R., Coath, C.D., Harrison, T.M., McKeegan, K.D., 1997. Prolonged residence times for the youngest rhyolites associated with Long Valley caldera: ion microprobe dating of young zircons. Earth and Planetary Science Letters 150, 27-38.

Sambridge, M.S., Compston, W., 1994. Mixture modeling of multi-component data sets with application to ion probe zircon ages. Earth and Planetary Science Letters 128, 373-390.

Schmitt, A.K., 2006. Laacher See revisited: high-spatial-resolution zircon dating indicates rapid formation of a zoned magma chamber. Geology 34, 597-600.

Schmitt, A.K., Wetzel, F., Cooper, K.M., Zou, H.B., Worner, G., 2010. Magmatic longevity of Laacher See Volcano (Eifel, Germany) indicated by U-Th dating of intrusive carbonatites. Journal of Petrology 51, 1053-1085.

Schmitz, M.D., Bowring, S.A., Ireland, T.R., 2001. Evaluation of Duluth Complex anorthositic series (AS3) zircon as a U-Pb geochronological standard: new highprecision isotope dilution thermal ionization mass spectrometry results. Geochimica et Cosmochimica Acta 67, 3665-3672

Simon, J.L., Renne, P. R., and Mundil, R., 2008. Implications of pre-eruptive magmatic histories of zircons for U-Pb geochronology of silicic extrusions. Earth and Planetary Science Letters 266, 182-194.

Sun, S.S. and McDonough, W.F. (1989). Chemical and isotopic systematics of oceanic basalts; implications for mantle composition and processes. In: Magmatism in the Ocean Basins. Saunders, A.D. and Norry, M.J. (Editors), Geological Society of London 42, 313-345.

Tucker, S. T. (2011) U-Th dating of zircons from a Holocene volcanic eruption (Dayingshan volcano, Tengchong volcanic field): Insight into magma chamber storage. Auburn University, MS thesis, 80pp.

Turner, S.P., Arnaud, N., Liu, J., Rodgers, N., Hawkesworth, C., Harris, N., Kelley, S., Van Calsteren, P., Deng, W., 1996. Post-collision, shoshonitic volcanism on the Tibetan Plateau: implications for convective thinning of the lithosphere and the source of ocean island basalts. Journal of Petrology 37, 45-71.

Wang, F., Peng, Z.C., Zhu, R.X., He, H.Y., Yang, L.K., 2006. Petrogenesis and magma residence time of lavas from Tengchong volcanic field (China): evidence from U series disequilibria and $^{40}Ar/^{39}Ar$ dating. Geochemistry, Geophysics, Geosystems 7, Q01002 10.1029.

Watson, E.B., Harrison, T.M., 1983. Zircon saturation revisited: temperature and composition effects in a variety of crustal magma types. Earth and Planetary Science Letters 64, 295-304.

Wendt, I., Carl, C., 1991. The statistical distribution of the mean squared weighted deviation. Chemical Geology 86, 275-285.

Wiedenbeck, M., Alle, P., Corfu, F., Griffin, W.l., Meier, M., Oberli, F., Vonquadt, A., Roddick, J.C., Speigel, W., 1995. 3 natural zircon standards for U-Th-Pb, Lu-Hf, trace-element and REE analyses. Geostandards Newsletter 19, 1-23.

Wilson, M., 1989. Igneous Petrogenesis: a Global Tectonic Approach. London (Unwin Hyman), 466 pp.

Yu, H.M., Lin, C.Y., Shi, L.B., Xu, J.D., Chen, X.D., 2010. Characteristics and origin of mafic and ultramafic xenoliths in trachyandesite lavas from Heikongshan volcano, Tengchong, Yunnan Province, China. Science in China (Earth Science) 53, 1295-1306.

Zhao, Y.W. and Fan, Q.C., 2010. Magma origin and evolution of Maanshan volcano, Dayingshan volcano and Heikongshan volcano in Tengchong area. Acta Petrologica Sinica 26, 1133-1140.

Zhu, B.Q., Mao, C.X., Lugmair, G.W., Macdougall, J.D., 1983. Isotopic and geochemical evidence for the origin of Plio-Pleistocene volcanic-rocks near the Indo-Eurasian collisionalmargin at Tengchong, China. Earth and Planetary Science Letters 65, 263-275.

Zou, H.B., 2007. Quantitative Geochemistry: Imperial College Press, London, 304 pp.

Zou, H.B. and Fan, Q.C., 2011. Uranium-thorium isotope disequilibrium in young volcanic rocks from China. Acta Petrologica Sinica 27, 2821-2826.

Zou, H.B., Reid, M.R., Liu, Y.S., Yao, Y.P., Xu, X.S., Fan, Q.C., 2003. Constraints on the origin of historic potassic basalts from northeast China by U-Th disequilibrium data. Chemical Geology 200, 189-201.

Zou, H.B., Fan, Q.C., Yao, Y.P., 2008. U-Th systematics of dispersed young volcanoes in NE China: asthenosphere upwelling caused by piling up and upward thickening of stagnant Pacific slab. Chemical Geology 255, 134-142.

Zou, H.B., Fan, Q.C., Schmitt, A.K., Sui, J.L., 2010. U-Th dating of zircons from Holocene potassic andesites (Maanshan volcano, Tengchong, SE Tibetan Plateau) by depth profiling: Time scale and nature of magma storage. Lithos 118, 202-210.